Accepted Manuscript

*Journal of the Geological Society*

# Concretionary cementation of a Scottish Middle Jurassic sandstone by hot, Paleocene fluids: a clumped isotope study

R.B. Paxton, J.E. Andrews, P.F. Dennis, A.D. Marca & C. Holmden

DOI: https://doi.org/10.1144/jgs2022-175

To access the most recent version of this article, please click the DOI URL in the line above. When citing this article please include the above DOI.

Received 13 December 2022
Revised 3 March 2023
Accepted 7 March 2023



Supplementary material at https://doi.org/10.6084/m9.figshare.c.6459860

# Concretionary cementation of a Scottish Middle Jurassic sandstone by hot, Paleocene fluids: a clumped isotope study

R.B. Paxton, J.E. Andrews* P.F Dennis, A.D. Marca and C. Holmden[1],

School of Environmental Sciences, University of East Anglia, Norwich, NR4 7TJ, UK

[1]Saskatchewan Isotope Laboratory, Department of Geological Sciences, University of Saskatchewan, Saskatoon, S7N 5E2, Canada.

*Corresponding author: email: j.andrews@uea.ac.uk

Running Header: Clumped isotopes in Middle Jurassic sandstone cements

## Abstract

This study focusses on new clumped isotope data from concretionary calcite cements in the Middle Jurassic Valtos Sandstone Formation (Great Estuarine Group) of the Inner Hebrides. Clumped isotopes show that concretion cementation began at 45±6 °C increasing to temperatures in excess of 70 °C before cooling slightly to 57 ± 7 °C at the concretion margin. In the early stages of cementation, calculated $\delta^{18}O_{FLUID}$ values were ~ –12‰ VSMOW, identical to an estimate of Paleocene Hebridean meteoric water based on hydrothermal reactions close to Paleocene Igneous Centres. These $\delta^{18}O_{FLUID}$ values imply that concretion cementation started in the Paleocene probably during the earliest stages of phreato-magmatic effusive igneous activity. As the concretion grew, temperature changes were accompanied by progressively evolving $\delta^{18}O_{FLUID}$ compositions up to +2.1 ± 1.1‰ VMOW. These evolving $\delta^{18}O_{FLUID}$ compositions were caused by isotope exchange reactions between $^{18}O$-rich lithologies and hot basinal fluids migrating upward along faults. This fluid flow was driven by progressive crustal loading from the thickening Paleocene lava pile which also caused sandstone compaction. Published radiometric dates that constrain the emplacement time of the Skye Lava Group, and its subsequent rapid erosion, suggest that concretion formation and final compaction was completed in no more than 2.6 myr, far more rapidly than modelled previously. Initial concretion growth that pre-dates development of volcanic topography shows that the strongly negative compositions of Hebridean Paleocene meteoric water are mainly of latitudinal rather than orographic origin.

Supplementary material: [clumped isotope data correction and uncertainties, sample details and additional figures] is available at http://doi.org/ xxx

## Introduction: Carbonate Concretions and Clumped Isotopes

Carbonate concretions are common features in sedimentary rocks (McBride, 1988, McBride et al., 2003; Wilkinson, 1991, 1992, 1993; Mozley and Burns, 1993; Selléz-Martínez, 1996; Raiswell and Fisher, 2000; and others). While mudstone-hosted concretions have typically initiated during microbially- mediated early diagenesis (e.g., Raiswell and Fisher 2000 and references therein), the formation mechanism and timing of sandstone-hosted concretions are much less-well understood: this is despite their importance in reservoir rocks where they can reduce porosity and impede fluid flow, lowering reservoir quality (e.g., Morad et al., 2010; Nyman et al., 2014). While reasons for nucleation, distribution (Bjørkum and Walderhaug, 1990) and growth rates (Wilkinson and Dampier, 1990) of sandstone-hosted concretions have been proposed, traditional geochemical approaches to understanding pore fluid evolution (e.g., Wilkinson 1993; Noh and Lee, 1999; McBride et al., 2003) have been limited because pore fluid compositions and the timing of cementation are not usually known. These limitations have thus required, reasonable, but usually unconstrained assumptions to enable interpretations.

With the advent of clumped isotope paleothermometry the requirement for assumptions about fluid $\delta^{18}O$ values has been removed (Ghosh et al., 2006). Furthermore, the abiotic sparry calcites that cement sandstones are excellent material for clumped isotope analysis, crystallising slowly under shallow to deeper burial conditions where temperatures >20 °C (Defliese &Lohmann, 2016; Purvis et al., 2020) ensure isotope exchange reaction rates are fast, and equilibrium between dissolved inorganic carbon (DIC)-calcite is attained (cf. Daëron et al., 2019).

Clumped isotopes have been used to investigate a number of sedimentary diagenetic scenarios including: investigating pore fluid sources and temperatures for cements in fault systems (e.g., Swanson et al., 2012; Bergman et al., 2013); identifying reactivation of syndepositional fracture networks in carbonate platforms (Budd et al., 2013), and to help better understand carbonate recrystallization and alteration (e.g., Huntington et al., 2011; Suarez and Passey, 2014; Sample et al., 2017; Stolper et al., 2018; Guo et al., 2021). Investigations of cementation specifically have included the utility of early meteoric diagenetic cements in paleoclimate studies (Defliese and Lohmann, 2016), and cementation histories in mudrock-hosted concretions (Loyd et al., 2012; 2014; Dale et al., 2014; Heimhofer et al., 2017; Paxton et al., 2021).

The application of clumped isotopes to carbonate cemented sandstones should significantly improve our understanding of the temperatures at which cementation

proceeded (e.g. Methner et al., 2016; Purvis et al., 2020; Cao et al., 2023), provide insights into porewater evolution during concretion growth (e.g., Fan et al. 2014), and help better constrain the burial depth of cementation through the link between temperature and geothermal gradients (e.g., Purvis et al., 2020; Cui et al., 2019; 2021; Jimenez-Rodriguez et al., 2022).

In this paper we present clumped isotope data from calcite cements in concretions from the Middle Jurassic Valtos Sandstone Formation of the Great Estuarine Group of the Inner Hebrides (Figs. 1 and 2). These concretions are well suited to such an approach, their age and geological context making them excellent analogues for diagenetic processes operating in subsurface Jurassic North Sea reservoirs. The sedimentology and diagenesis of the sandstone have been studied extensively (Hudson, 1964; Harris and Hudson, 1980; Tan and Hudson 1974; Harris, 1992; Hudson and Andrews, 1987; Wilkinson 1992; 1993) and models for concretion growth offered (Wilkinson and Dampier 1990; Wilkinson, 1993). However, until now the diagenetic interpretations have relied on a number of assumptions regarding the burial temperature (and depth) of concretion growth and $\delta^{18}O$ values of pore fluids from which the calcite cements formed (Hudson and Andrews, 1987; Wilkinson, 1993). With the clumped isotope temperatures of concretionary calcite cement determined in this study, we are now in a position to calculate pore fluid $\delta^{18}O$ values from which the cements precipitated using an appropriate palaeotemperature equation (Epstein et al., 1953; Craig 1965; Anderson & Arthur, 1983; Kim & O'Neil, 1997), thus enabling more rigorous testing of diagenetic models (combined fluid, burial and temperature histories) of concretion growth in the Valtos sandstone. The approach and results should prove instructive for wider studies on sandstone cementation.

## Valtos Formation Geological Setting

The Bathonian Valtos Sandstone Formation (hereafter Valtos Formation; Fig. 1) is a thick sandstone unit of fluvio-deltaic origin (Harris, 1992), intercalated into the mainly muddy and sandy sediments of the Great Estuarine Group (GEG). Fossils in these sediments mostly indicate a low salinity, brackish and occasionally marginal-marine lagoonal setting (Hudson, 1963; 1980). Deposition was focussed in two half graben, the Sea of the Hebrides and the Inner Hebrides Basins, best defined by the deltaic sandstone units, the older Elgol Sandstone Formation (Harris and Hudson, 1980; Harris, 1989) and the younger Valtos Formation (Fig. 1).

The Valtos Formation outcrops on the Isles of Skye, Raasay, Eigg and Muck (Fig. 2) with some lateral variation between localities (Harris and Hudson, 1980). In this work

we concentrated on metre-scale spherical concretions from the type section (Harris and Hudson, 1980) at Valtos, in Trotternish (N. Skye) and from Laig Bay on Eigg (Harris, 1992). The Valtos Formation lithologies are broadly medium/coarse grained concretionary sandstones often containing a small, brackish-tolerant, burrowing bivalve (*Neomiodon* sp.; Hudson, 1963; 1980). Sandstone units are typically capped by *Neomiodon* biosparite limestones, with further *Neomiodon* limestones and silty shales interbedded with the sandstones (Harris and Hudson, 1980). *Neomiodon* shells were aragonite, and some original aragonite is preserved in shells deposited in mudstones (Hudson and Andrews, 1987), but in the sandstones they are only found as neomorphic calcite within calcite cemented concretions or limestone beds. The surrounding uncemented/lightly cemented sandstones are unfossiliferous (Hudson and Andrews, 1987), suggesting that here total bioclast dissolution occurred.

Near the base of the Valtos type-section (bed 3 of Harris and Hudson, 1980), just above a lower tabular concretionary unit, spherical concretions >1 m in diameter occur (Figs 3 & S1), which are the primary focus at this locality; however, we also sampled a concretion higher in the sequence. At Laig Bay on Eigg we again sampled metre-scale concretions in Division E (Hudson and Harris, 1979; Harris, 1992) toward the top of the formation (Fig. S2). At both Valtos and on Eigg we also sampled veins of calcite that cross-cut (post-date) the concretions, Some calcite veins and decimetre wide zones of nodular cements also post-date Paleocene igneous dykes, being common sub-parallel to dyke margins on Eigg (Figs 4 & S3) and filling fractures within a dyke at Valtos (Fig. S4). Details of all sample locations are given in the Supplementary Material.

The burial history of the GEG has been discussed by Hudson and Andrews (1987) and Morton (1987) and is updated and summarised in Figure 5. Briefly, the GEG was buried <500 m prior to uplift before the Late Cretaceous (Hudson, 1983; Morton, 1987), probably between 140–130 Ma (Fig. 5) based on apatite fission-track analysis (AFTA; Holford et al., 2010). Evidence for significant sedimentation in the Upper Cretaceous is lacking and preserved outcrops do not exceed ~25 m thickness (Hudson, 1983; Harker 2002). A phase of early Cenozoic uplift and erosion between 65-60 Ma (Holford et al., 2010) combined with ongoing eustatic sea-level fall in the Maastrichtian-Danian (Haq, 2014), removed most of the thin Upper Cretaceous sediment and in places exposed underlying Jurassic rocks as a regolith (Fig. 5).

In the Paleocene, regional igneous activity associated with the British Tertiary magmatic province buried the Mesozoic sediments rapidly (within 1.6 Ma; Hamilton et al., 1998) under hundreds of metres of lavas; the Trotternish lava pile is estimated ~1200 m

thickness (England, 1994; Emeleus and Bell, 2005). Intrusive sills and dykes were also emplaced during this igneous activity, including the Little Minch Sill complex of Trotternish, emplaced sometime after lava deposition (Gibson, 1990; Emeleus and Bell; 2005), while dyke emplacement probably occurred throughout the igneous event (England, 1994; Emeleus and Bell, 2005).

The Skye Central Complex post-dates emplacement of the Skye Lava Group (Emeleus and Bell, 2005) and its thermal effects are spatially limited (Fig. 2) to a hydrothermal alteration zone about 6.5 to 10 km out from the centre of the complex (Taylor and Forester, 1971; Forester and Taylor, 1977; Lewis et al., 1992). Outside this zone, the thermal effects of localised contact alteration on Jurassic sediments are surprisingly limited and easy to recognise in localities where they have occurred. Organic matter in unaltered Jurassic rocks is extremely immature (Thrasher, 1992; Lefort et al., 2012), with some vitrinite reflectivity ($R_0$) values well below 0.5% (Hudson and Andrews 1987; Fyfe et al., 2021); in mudrocks, molluscan aragonite is still preserved (Hudson and Andrews, 1987; Holmden and Hudson, 2003). In such immature shales, the thermal influence of smaller igneous intrusions on organic maturity is typically proportional to intrusion width (Bishop and Abbott, 1995) and marked in the field by darker coloration and decreased shale fissility. However, in parts of east Trotternish, particularly around Lealt and south of Staffin, intrusions of the Little Minch Sill Complex are thick and numerous enough to have caused substantial local thermal alteration.

$R_0$ values <0.5% in some samples of the Lealt, Duntulm and Kilmaluag Formations of the GEG in Trotternish suggest burial temperatures around 50 °C (see also Hudson and Andrews 1987) while analcime zone zeolites from the lowest part of the Trotternish lava pile (resting on GEG sediments; King 1976) suggest local post-lava hydrothermal temperatures between 75 °C to 90 °C. There is no evidence that this hot water penetrated the clay-rich formations of the GEG. AFTA maximum temperatures from the GEG of N. Skye are between 85 ± 10 °C to ≥110 ± 10 °C (Holford et al., 2010), but measured only in the sandstones of the Valtos and Duntulm Formations. The likelihood of our samples having undergone post-depositional solid-state bond reordering (Henkes et al. 2014; Passey and Henkes 2012; Shenton et al. 2015; Stolper and Eiler, 2015; Hemingway & Henkes, 2021) is low; such resetting in calcite typically requires subsurface temperatures in excess of 100 °C for more than 100 myr, which for the GEG is not possible, except where local igneous thermal alteration occurred.

Concretion Petrography

The large spherical concretions formed from a single generation of ferroan calcite, with no inter crystal zoning (Wilkinson, 1993), growing concentrically outward from an (assumed) initial nucleus. At the centre of the concretion, crystals are equant, ~ 0.25 mm wide, and increase in both size and elongation radially to >50 mm (Wilkinson, 1993), with a poikilotopic texture that is clearly visible in hand specimen. *Neomiodon* shells are preserved as neomorphic calcite and the amount of shell material preserved decreases from centres to the edges of concretions (Wilkinson, 1993). Pressure dissolution of shells is common, some being reduced to 'films' between quartz grains (Hudson and Andrews, 1987). As shells are only preserved within concretions, pressure solution must have occurred before concretionary cementation (Hudson and Andrews, 1987). Point counting (Wilkinson, 1989) shows that the host sandstone retains ~30% porosity (minus-cement porosity), reduced from an estimated original porosity of 45-50%. At Valtos, some concretions show compaction of thinly bedded host sediments around their margins (Fig. 3B). This indicates that some burial compaction continued after concretion growth (Hudson and Andrews, 1987; Wilkinson, 1993); the host sandstone framework being ~20% more compacted than the concretions (Wilkinson, 1993). Curiously, other concretions show no clear evidence of post-concretion compaction.

**Methods**

Samples were taken where the sandstones showed no visible or petrographic/geochemical evidence of thermal alteration. Sandstone calcite cements from the concretions, vein-filling sparry calcite and calcite amygdales in lavas were drilled from fresh surfaces taking care to avoid heating and pressure. Core plugs of concretion VR1 (NG 516 642; Fig. S1) were re-sampled along the vertical transect of Wilkinson (1993). For each VR1 measurement between 9.45-10.19 mg of sample was reacted, in order to achieve a gas volume proportionate to the yield of a pure carbonate sample of 4 mg. All VR1 samples were measured 3-4 times and sample M8605 was analysed once each day (10 measurements) to establish a representative distribution of error. Most non-VR1 samples were also analysed as 4 mg or 4 mg gas yield equivalent although some were measured as 6 mg or equivalent gas yield; the larger resulting gas volumes from 6 mg did not affect the resulting $\Delta_{47}$ values.

Samples were digested in a common acid bath containing ~105% phosphoric acid heated to 87°C. The released $CO_2$ was dried by sublimating at ~ -115°C, then passing through two spiral traps held at -115°C, freezing with liquid nitrogen into a manometer.

Potential hydrocarbon and chlorocarbon contaminants were removed by cryodistilling through a 12 cm x 4 mm i.d. glass tube packed with Porapak Q ion exchange resin and held at −20°C. The resultant gas was transferred directly to the mass spectrometer. Full details of the gas preparation are in Paxton (2022).

Sample $CO_2$ was analysed for $\delta^{45}$ - $\delta^{49}$ on the MIRA dual-inlet isotope ratio mass spectrometer (IRMS) at the University of East Anglia (UEA), using the operating and data handling protocol detailed in Dennis et al. (2019). Carbonate standards ETH1, ETH3 and UEACMST were also prepared and measured every day to provide an estimate of long-term measurement uncertainty, and to determine the transfer function between the local reference frame and the carbon dioxide equilibrium scale of Bernasconi et al. (2018), '$\Delta_{47}$ (CDES-25)'. $\Delta_{47}$ values used for ETH1 and ETH3 at 87°C acid digestion were empirically derived at UEA; ETH1 = 0.218‰, and ETH3 = 0.613‰. If projected to represent acid reaction at 90°C, transfer functions created using the UEA derived ETH values versus those from Bernasconi et al. (2021) produced sample $\Delta_{47}$ (CDES-90) values that were within measurement error of one another. To convert $\Delta_{47}$ values derived by reaction at 87°C to '$\Delta_{47}$ (CDES-25)', an acid fractionation factor of 0.062‰, empirically determined at UEA, was added.

For Sr isotopes, carbonate powders were dissolved in twice the stoichiometric volume of 1.0 N HCl required to completely dissolve the sample. After the effervescence ceased, the solution was centrifuged, and the supernatant was separated from any residues and dried down on a hot plate. The sample was purified from Ca, Rb and other trace elements using conventional cation exchange chromatography. The purified Sr aliquot was then loaded onto single Ta filaments with phosphoric acid and Ta-gel to increase the ionization efficiency of Sr in the mass spectrometer. The $^{87}Sr/^{86}Sr$ measurements were performed using a thermal ionization mass spectrometer (Thermo-Elemental Triton instrument) operating in static multi-collection mode. An exponential law was used to correct the measured $^{87}Sr/^{86}Sr$ ratios for instrumental mass fractionation against measurements of $^{88}Sr/^{86}Sr$ with a true ratio of 8.375209. Isobaric interference of $^{87}Rb$ on $^{87}Sr$ was monitored using $^{85}Rb$, and corrections made if necessary. The external reproducibility of $^{87}Sr/^{86}Sr$ is better than ±15 ppm (2σ), based on multiple runs of SRM 987 performed throughout the course of this work, which yielded a mean $^{87}Sr/^{86}Sr$ ratio of 0.710259.

Temperature calculation

Equation 1, empirically derived at UEA (Kirk, 2017; Dennis et al., 2019), was used to calculate the formation temperatures of each carbonate sample:

$$\Delta_{47(CDES25)} = \frac{(0.0389 \times 10^6)}{T^2} + 0.2139 \quad \text{Equation 1}$$

Where T = temperature in Kelvin.

The calcite-water isotope fractionation factor calibration of Kim and O'Neil (1997) was used for all samples, being appropriate for abiotic calcite cements. The measurement uncertainty for $\delta^{18}O_{CARBONATE}$, $\delta^{13}C$ and $\Delta_{47}$ is reported as ± 1 standard error of the pooled standard deviation unless stated otherwise. Pooled standard deviation was used wherever sample compositions were similar.

Temperature and $\delta^{18}O_{FLUID}$ values were calculated using the mean $\Delta_{47}$ and $\delta^{18}O_{CARBONATE}$ values with full propagation of the measurement and calibration uncertainties. The $\delta^{13}C_{CARBONATE}$ and $\delta^{18}O_{CARBONATE}$ values are reported on the Vienna-Pee Dee Belemnite (VPDB) scale and $\delta^{18}O_{FLUID}$ values on the Vienna-standard mean ocean water (VSMOW) scale. All data, calculations, sample replicates and pooled standard deviation-derived standard errors are given in the Supplementary Material.

## Results

Stable, clumped and Sr isotope results for all samples are given in Tables 1 and 2 and plotted on Figures 6-8. Here we describe the clumped isotope data for the large concretion VR1 at Valtos in detail, as this (Table 1 and Fig. 6) helps to frame the discussion of other samples. From the centre to the edge of VR1 (Fig. 6), covarying changes in measured $\Delta_{47}$-derived temperatures and calculated pore water $\delta^{18}O$ values follow the zonal pattern of changing $\delta^{18}O_{carbonate}$ values identified by Wilkinson (1993). In Zone 1 (0–35 cm), $\Delta_{47}$-derived temperatures are 45 ± 6 °C at the centre of the concretion (0-24 cm), increasing to ~50 °C between 24 and 31.5 cm. The corresponding $\delta^{18}O_{FLUID}$ values are between –11.1 ± 1.1‰ and –12.6 ± 1.1‰ VSMOW, increasing to –7.7 ± 0.9‰ VSMOW near the edge of Zone 1. In Zone 2 (40–55 cm) $\Delta_{47}$-derived temperatures increase to 63 ± 8 °C, with a peak value of 73 ± 8 °C. The corresponding $\delta^{18}O_{FLUID}$ values range between 0.0 ± 1.2‰ and +2.1 ± 1.1‰ VSMOW. The temperature slightly decreases to 57 ± 7 °C in Zone 3 (~58 cm to 60.5 cm), the outer part of the concretion with $\delta^{18}O_{WATER}$ values decreasing, as well, to –4.4 ± 1.1‰ VSMOW (Fig. 6).

For comparison, a concretion from bed 38 (Dun Dearg, Valtos cliffs) gave a $\Delta_{47}$-derived temperature of 64 ± 9 °C and a $\delta^{18}O_{FLUID}$ value of –1.8 ± 1.4‰ (Table 1 and Fig. 7), which is like Zone 2 in VR1. In another example, the centre of a large concretion on Eigg gave a $\Delta_{47}$-derived temperature of 79 ± 8 °C, and a $\delta^{18}O_{FLUID}$ value of +4.9 ± 1.1‰ VSMOW, which is also reminiscent of Zone 2 in VR1. However, 63 cm further from the

centre of this concretion, the temperature increased to 98 ± 9 °C and $\delta^{18}O_{FLUID}$ value increased, as well, to +7.2 ± 1.2‰ (VSMOW) which is more extreme than observed in Zone 2 in VR1, while the outermost sample from this concretion gave a temperature of 68 °C, and $\delta^{18}O_{FLUID}$ value of +2.7 ± 1.1‰ (VSMOW) (Table 1 and Fig. 7).

Other examples of calcite sparry cement data from the Valtos Formation on Skye and Eigg are also shown on Figure 7. Most calcite cements in veins and vugs that post-dated concretions at Valtos gave temperatures between 30 ± 13 °C to 52 ± 10 °C and $\delta^{18}O_{FLUID}$ values between –12.1 ± 2.7‰ and –15.4 ± 2.5‰ VSMOW. Exceptions include a vein from the base of a large concretion (189-1; Table 1) which gave a temperature of 67 ± 10 °C and a $\delta^{18}O_{FLUID}$ value of +4.1 ± 1.5‰ VSMOW and a vein from the margin of a Tertiary dyke (189-6; 24 ± 8 °C; -16.5 ± 1.6‰ VSMOW). On Eigg, a nodular concretion from a cemented sandstone horizon adjacent to a Paleocene dyke margin (169-1; Table 1) gave a temperature of 42 ± 9 °C and fluid value of –14.6 ± 1.7‰ VSMOW, comparable with veins from the Valtos that post-date dyke intrusion.

$\delta^{18}O_{FLUID}$ values for Paleocene Hebridean meteoric waters that post-dated lava emplacement and cooling were calculated from calcite amygdales in the Eigg Lava Formation (SA-1 and SA-2). The $\Delta_{47}$ temperatures were within error at 28 ± 6 °C and 27 ± 6 °C, with $\delta^{18}O$ fluid values (–13.7 ± 1.2‰ and –15.1 ± 1.1‰ VSMOW) comparable to the more negative values in the concretions and vein calcites (Table 1 and Fig. 7). These samples gave the lowest $\delta^{13}C$ values measured in this study (–6.1‰ and –5.8‰ VPDB) while $\delta^{18}O_{CARBONATE}$ values of –16.6 ± 0.1‰ and –17.8 ± 0.1‰ VPDB are comparable to many of the calcite cements measured here.

## Discussion

### Concretion VR1

Horizontal and vertical centre to edge geochemical transects from concretion VR1 (Wilkinson 1993) indicated that the concretion grew concentrically. The cement was assumed to derive from the redistribution of calcium carbonate from dissolution of originally aragonite *Neomiodon* shells. This is supported by the preservation of shell debris within concretion bodies but not in the host sands (Tan and Hudson, 1974; Hudson and Andrews, 1987) and by the reduction in shell material from concretion centres to edges (Wilkinson, 1993).

The initial cementation in Zone 1 (~14% of concretion volume) had calcite cement $\delta^{18}O$ as low as –18.2‰ (Figs 6A and S5), values that were difficult to explain in

Wilkinson's favoured model of concretion growth under a stable burial temperature. In Zone 2 (~53% of concretion volume) the cements had increased Mg and Fe contents (Fig. S6) while $\delta^{18}O_{CARBONATE}$ transitioned to higher values (Wilkinson, 1993). In zone 3 (~33% of concretion volume), the outermost part, cement $\delta^{18}O_{CARBONATE}$ decreased again (Fig. 6A) along with both Mg and Fe content. The new $\Delta_{47}$-derived temperatures and $\delta^{18}O_{FLUID}$ compositions (Fig. 6B and C) clearly record the zonal centre to edge changes identified by Wilkinson (1993). This range in temperatures in a single concretion is incompatible with a stable burial temperature model and rules out post-depositional solid-state bond reordering (Passey and Henkes 2012; Henkes et al. 2014; Shenton et al., 2015; Stolper and Eiler 2015; Hemingway & Henkes, 2021).

*Zone 1: Early cementation*

The initiation of cementation was thought by Wilkinson (1993) to be due to an influx of meteoric water into the sand body that reduced (by dilution) any Mg inhibition to calcite nucleation in the connate pore fluids (Wilkinson, 1993). Meteoric water flushing was assumed to have been a Mid-Late Jurassic event or due to recharge after uplift in the Cretaceous (Wilkinson, 1993). $\delta^{18}O_{FLUID}$ values of ~ –12‰ VSMOW from the centre of concretion VR1, while consistent with a meteoric water source (e.g., Dansgaard, 1964), are much more negative than traditionally estimated Hebridean values of Jurassic meteoric water (between –4 to –7‰ VSMOW; Hudson and Andrews, 1987; Searl, 1992). Such estimates are incompatible with the Z1 $\Delta_{47}$-derived $\delta^{18}O_{FLUID}$ values ~–12‰ VSMOW.

There is no direct evidence of meteoric cementation in the sparse Inner Hebridean Cretaceous sediments which in the study area are largely of Turonian age (Harker 2002); this precludes measurements or inferences regarding pore fluid composition. Cretaceous meteoric water recharge could have occurred between 140–130 Ma following uplift (Holford et al. 2010), but there is no concrete evidence for it. Elsewhere in the UK, Hendry (1993) interprets pore-filling cement in English midlands Middle Jurassic limestones, to have formed from Early Cretaceous meteoric water with $\delta^{18}O$ more negative than –8‰ VSMOW. Climatic models for Hebridean Middle Cretaceous palaeolatitudes also suggest negative $\delta^{18}O$ values between –5.5 and –11‰ VSMOW (Table 3 and references therein). We therefore cannot rule out the possibility that Z1 cementation in concretion V1 was from pore fluids sourced from isotopically negative meteoric water during a period of pre-upper Cretaceous exposure.

The involvement of meteoric water in hydrothermal reactions in zones around the Paleocene igneous centres allowed Taylor and Forester (1971) and Forester and Taylor (1977) to calculate the $\delta^{18}O_{fluid}$ composition of the Paleocene meteoric water as –12‰ VSMOW. These low values were corroborated by Fallick et al. (1985) and by the new clumped isotope data reported in this study (Table 1) from the Eigg Lava Formation calcite amygdales ($\delta^{18}O$ values of –13.7 ± 1.2‰ and –15.1 ± 1.1‰ VSMOW). There is thus direct evidence that VR1 initiation may have commenced from isotopically negative Paleocene pore fluids.

There are several widely dispersed localities where Paleocene lava was emplaced directly onto a land surface where the Valtos Formation sandstone was outcropping (Fig. 2), including the east coast of Eigg, in the Upper Glen 1 borehole in Waternish (NG299506; see Schofield, 2016; Fyfe et al., 2021), on Raasay (NG577430), at Craig Ulatoa near Prince Charles' Cave in Trotternish (NG51047) and in Strathaird (NG553211) where the Valtos Sandstone is directly overlain by a meteoritic ejecta layer (Drake et al., 2018) of similar age to the overlying lavas. At Waterstein Head on Waternish the lavas are just above the Valtos Formation. These outcrops demonstrate that parts of the Valtos sandstone aquifer were completely unroofed by erosion, basinwide, exposing multiple points of entry (others may be present in sub-crop) for meteoric-derived fluids to enter the aquifer. Moreover, as fragmentary outcrops of thin, marine, Upper Cretaceous sediments are known close to a number of these localities (Hudson, 1983), it is very likely that this phase of erosion post-dated Upper Cretaceous deposition (Fig. 5), driven by Paleocene (65-60 Ma) uplift (Holford et al., 2010) accompanied by ongoing eustatic sea-level fall in the Danian (Haq, 2014).

Cementation of Z1 occurred at around 47 °C and it is unlikely that much of this heat was related to burial (cf. Wilkinson, 1993), given that parts of the sandstone were demonstrably at land surface with maximum burial probably less than the thickness of the sandstone itself (i.e., ~100 m in Trotternish). However, if Z1 cementation was concurrent with Paleocene igneous activity, local sources of heated water would have been common, even before lava emplacement. The earliest evidence for volcanic activity in N. Skye is from the Portree Hyaloclastite Formation (Anderson and Dunham, 1966; Bell and Williamson 2002), which while not dated radiometrically, is not likely to be much younger than 60.53 ± 0.08 Ma (the age of the Rum basic/ultrabasic pluton (Hamilton et al., 1998), clasts of which are found in the Skye Lava Group). Phreato-magmatic vent volcanism (Anderson and Dunham, 1966) during sub-aqueous tuff and hyaloclastite deposition explains how heated groundwater may have locally accessed and migrated into the porous Valtos Sandstone aquifer. The Z1 $\delta^{18}O_{FLUID}$ values begin around –12‰ in the concretion

centre changing to –11‰ VSMOW (Table 1), values that are identical to, or not much evolved from, previously estimated meteoric-water compositions of –12‰ VSMOW (Taylor and Forester 1971; Forester and Taylor, 1977); they imply a near open system (high water/rock ratio) for oxygen isotopes. The Krafla geothermal system on Iceland is a modern isotopic analogue, where meteoric groundwater ($\delta^{18}O_{FLUID}$ ~ –12‰ VSMOW) is heated in basaltic rocks under high water/rock ratios, resulting in only small changes to the measured hydrothermal fluid $\delta^{18}O$ (Pope et al., 2009, 2010).

*Zone 2*

The transition of $\delta^{18}O_{CARBONATE}$ from –18.5‰ to –8.6‰ is caused by a change in both temperature and $\delta^{18}O_{FLUID}$ composition (Fig. 6) and not simply a change in pore fluid compositions as envisioned by Wilkinson (1993).

The $\Delta_{47}$-derived temperature change between outermost Z1 and innermost Z2 is from 53 ± 3 °C to 79 ± 7 °C and is most simply explained by the introduction of heated water, with temperature sustained around 70-80 °C for the duration of the cement precipitation in Z2, accounting for over half the volume of the concretion. The temperature change is preceded, and then accompanied, by a change in $\delta^{18}O_{FLUID}$ composition (Fig. 6); Z1 averages –11.1‰ VSMOW, whereas Z2 averages +0.9‰ VSMOW, a 12‰ change, with highest values of +2.1 ± 1.1‰ VSMOW at the edge of Z2. There is also a marked increase in calcite Fe and Mg content (Wilkinson, 1993; Fig. S6) that follows the temperature and $\delta^{18}O_{FLUID}$ trends. The meteoric pore fluid of Z1 must have been replaced by a pore fluid that was relatively enriched in $^{18}O$. Despite the sharp geochemical change between zones there is no evidence for a pause in cementation; only a single generation of ferroan calcite is present (Wilkinson, 1993) although the crystals become more elongated in Z2. The $\delta^{18}O_{FLUID}$ composition then evolved progressively to more positive values over time.

Heated fluids in hydrothermal systems are known to undergo isotope exchange with surrounding rock units, and such water-rock interactions result in more positive $\delta^{18}O_{FLUID}$ values after exchange with $^{18}O$-rich country rocks (Craig, 1963; Sheppard, 1986). In the case of the Valtos Formation concretions the underlying country rocks are mainly Middle and Lower Jurassic mudrocks and sandstones, while the overlying country rocks are Middle and Upper Jurassic mudrocks and sandstones followed by Paleocene basalts. Skye basalts have $\delta^{18}O$ values above +5‰ SMOW (Taylor and Forester, 1971; Forester and Taylor, 1977) while mudrocks in the upper Great Estuarine Group have $\delta^{18}O$ values between +10 and +17‰ SMOW (Hamilton et al., 1992).

If Z1 cementation was concurrent with Paleocene igneous activity, it is logical to attempt to explain the progressive positive change in pore fluid values towards the outer part of the concretion as a result of meteoric water percolating through, and reacting with, hot basaltic lavas. However, we cannot find any evidence to support the notion that such reactions could achieve the magnitude of oxygen isotopic exchange required, i.e. to alter pore fluid $\delta^{18}O$ from –12‰ (Paleocene meteoric water) to +2‰ (Z2 fluid) VSMOW. In the Icelandic Reykjanes geothermal system, there is oxygen isotopic exchange between fluid and host basalts that results in hydrothermal fluid $\delta^{18}O$ around +2‰, but this happens largely from an initial seawater fluid source (Pope et al., 2009, 2010).

The alternative is that hot basinal fluids, enriched in $^{18}O$ by reaction with host basinal sediments, particularly mudrocks, migrated upward. There is now growing clumped isotope characterization of such basinal fluids with temperatures and $\delta^{18}O_{FLUID}$ values similar to those attained in our Z2 (e.g. Swart et al., 2016; Mangenot et al., 2018a; Dennis et al., 2019). In this scenario, basinal fluid flow was promoted by the progressive crustal loading of the thickening Paleocene lava pile. A kilometre thickness of lava emplaced within 1.6 Ma; Hamilton et al., 1998) would rapidly increase lithostatic pressure (~25 MPa). In confined sediments this could promote failure of over-pressured mudrock units to release a significant volume of fluid (Cathles & Smith 1983; Cathles & Adams 2005) that then flowed upward along faults (cf. Wilkinson 1993) into the Valtos Formation. The main phase of basinal-fluid cementation in Middle Jurassic sediments of the Paris Basin show broad similarity in $\Delta_{47}$-derived temperature characteristics and $\delta^{18}O_{FLUID}$ values, albeit the latter influenced by Triassic brine contributions (Mangenot et al., 2018a). The Valtos basinal fluids initially mixed with, but then gradually displaced the Z1 meteoric fluids explaining the progressive change to heavier $\delta^{18}O_{FLUID}$ values through Z2 and possibly influencing (elongating) cement crystal morphology.

This scenario also explains why the Z2 cements have high Fe and Mg contents (about 1.5x higher) relative to Z1. Both elements will be relatively easily leached from mudrocks, ferrous Fe solubility promoted by reducing and hot conditions (Garrels and Christ, 1965; Seyfried et al., 1991). The Z2 Fe contents are approximately 3x, and the Mg contents approximately 8x, those in limestone-hosted sparry calcite burial cements from the overlying Duntulm Formation (cf. Andrews 1986; Hudson and Andrews 1987). Basinal fluid temperatures of 70-80 °C suggest generation in mudrock units well below the GEG in the Lower Jurassic succession (see Morton 1987). For example, the Pabbay Shale Formation (Hesselbo et al., 1998) is likely to have been buried to around 2 km depth in north Skye and Waternish (Fyfe et al., 2021), and its pore fluids are likely to have been of marine or modified marine origin. There is no reliable data on the Paleocene geothermal

gradient but in the Upper Glen borehole (Fig. 1) vitrinite $R_0$ values between 0.7-0.8% are recorded in the Lower Jurassic Pabbay and Broadford Formations (Fyfe et al., 2021), values that are consistent with burial temperatures ~80 °C.

Taking all the evidence together it seems likely that, while Z1 of concretion VR1 began forming during the earliest stages of effusive igneous activity on Skye, Z2 was forming as the lava pile thickened. This must have occurred after 60.53 ± 0.08 Ma (see above) but before 58.91 ± 0.07 Ma (a date on Cuillin Gabbro; Hamilton et al., 1998), which post-dates extrusion of the Skye Lava Group). While concretion VR1 was growing the down-bearing pressure of the lava pile was initially not enough to overcome the supporting litho-and hydro-static pressure in the sandstone. At some stage the lava pile was thick enough to initiate sandstone burial compaction, at least some of which occurred after the concretion had formed. Concretion growth was probably complete before eruption of the Skye Central Complexes, that post-date eruption of the Skye Lava Group (Emeleus and Bell, 2005). This chronology rules out the possibility that the Z2 fluids are related to hydrothermal systems developed around the central igneous complex of Skye (Taylor and Forester, 1971; Forester and Taylor, 1977; Schofield et al., 2016). Similarly, influence of heat from intrusion of the Little Minch Sill complex into the Valtos Formation at Valtos cannot have been responsible for local fluid heating during concretion growth because the intrusion was emplaced after the Skye Lava Group (Anderson and Dunham, 1966; Gibson and Jones, 1991; Emeleus and Bell, 2005).

Three Sr isotope measurements from VR1 cements (Table 2 and Fig. 8) were used to investigate whether the calcites retained any isotopic fingerprint of fluid interaction between basinal sediments or lavas. All of the VR1 data (Fig. 8) is much less radiogenic than GEG clays (Hamilton et al., 1992) and more radiogenic than the lava values (Scarrow, 1992). The VR1 data are closest to values for GEG shells and other carbonates (Holmden and Hudson, 2003; Andrews et al., 1987). This outcome implies that both heated meteoric-water and basinal fluids were undersaturated with respects to aragonite, allowing them to dissolve aragonite shells encountered in the basinal sediments and/or as they entered the sandstone (Wilkinson, 1993), the shell-derived Sr overprinting any sediment or lava signature. This is supported by the $\delta^{13}C$ and Sr contents of the cements (Table 1 and Fig. S6), which also have rock buffered values derived from shell dissolution (Wilkinson, 1993).

*Zone 3*

Cements in Z3 lithify 30% (by volume) of VR1 in a relatively thin outer zone where we have a single $\Delta_{47}$ value (Table 1 and Fig. 6). This shows there is a change in $\Delta_{47}$-derived temperature and $\delta^{18}O_{FLUID}$ between Z2 and Z3, in addition to decreases in $\delta^{18}O_{CARBONATE}$, Mg and Fe contents (Wilkinson, 1993). The last temperature from Z2 is 73 ± 7 °C, which decreases to 57 ± 7 °C in Z3. The Sr isotope value for Z3 cement is not different to those from Z1 or Z2, which implies dissolving *Neomiodon* shells were still the main carbonate source. The Z3 fluid was clearly cooler and its $\delta^{18}O_{FLUID}$ value (–4.4 ± 1.1‰ VSMOW) indicates it contained less rock-derived $^{18}O$, and dissolved Fe and Mg. This suggests that the basinal fluid source was decreasing and possibly mixing with meteoric fluids that were penetrating the lava pile through fractures. High levels of seasonal meteoric precipitation (1175 mm to 2267 mm) are indicated by fossil flora preserved within the Skye Lava Group (Poulter, 2011). This mixed fluid had a composition that promoted the development of poikilotopic calcite crystals.

Cements from a sandstone-hosted concretion (EG191015-1; Table 1) from Dun Dearg (Valtos cliffs, bed 38 of Harris and Hudson, 1980), stratigraphically about 40 m above VR1 gave a $\Delta_{47}$-derived temperature of 64 ± 9 °C, and a $\delta^{18}O_{FLUID}$ value of –1.8± 1.4‰ VSMOW (Fig. 7). These values are similar to those from Z2 of concretion VR1 (Fig. 7) suggesting this phases of ferroan spar cementation was essentially coeval with the main growth phase of VR1.

Large concretion from Valtos Formation on Eigg

To better understand the significance of the VR1 data in a basin-wide context we studied a large spherical concretion at Laig Bay (Isle of Eigg), 75 km south of Valtos (Fig. 2). While this concretion is similar to VR1 it comes from near the top of the formation Division E (Harris and Hudson, 1980), rather than the base. Three measurements, roughly centre, intermediate, outer edge (Fig. S2) from this concretion gave values between 68 ± 7 °C to 98 ± 9 °C, and isotopically enriched pore fluid $\delta^{18}O$ between +2.7 ± 1.1‰ and +7.2 ± 1.2‰ VSMOW (Table 1 and Figs 6 and 7), comparable to those from Z2 in concretion VR1. They indicate that the high temperature, isotopically-enriched basinal pore fluids were widespread, both throughout the basin and throughout the thickness of the Valtos Formation. However, there is no evidence so far for an equivalent of the earlier Z1 meteoric fluids on Eigg, either in our data or inferred from data in Wilkinson (1992).

Vein cements that post-date large concretions

To put the VR1 and the Eigg concretion data into a wider paragenetic context, we discuss here clumped isotope data from vein-fed sparry calcite cements that post-dated concretion formation (Table 1 and Fig. 7).

The first (189-1; Valtos), cross-cuts a concretion ~2 m diameter from the same horizon as VR1 and gave a $\Delta_{47}$ temperature of 67 ± 10 °C and a derived $\delta^{18}O_{FLUID}$ value of +4.1 ± 1.5‰ VSMOW. These results are similar to those of Z2 in concretion VR1 (Fig. 7), indicating that a hot, evolved fluid was still accessing some fractures. The $\delta^{13}C$ is 0.1‰ VPDB, consistent with carbon sourced from dissolving *Neomiodon* shells.

The second vein samples come from the margins and interior of a small dolerite dyke at Valtos (Fig. S4), about two metres from 189-1. These veins are the fills of intrusion-parallel fractures that opened sometime (unconstrained) during or after cooling and contraction of the dyke and probably postdate concretion formation by hundreds of thousands of years. Samples 189-5v and 189-7a (Table 1) come from two generations of calcite that filled a fracture 5 cm wide within the dyke, while sample 189-6 comes from a 2-5 mm thick vein filling a fracture between the wall of the dyke and the host sandstone. Samples 198-5v and 189-6 gave $\Delta_{47}$ temperatures of 52 ± 10 °C and 40 ± 10 °C with pore fluid values of –12.7 ± 1.7‰VSMOW and –13.8 ± 1.9‰ VSMOW respectively. The former (189-5v) calcite is intergrown with a brown fibrous smectite (possibly saponite) as identified by X-Ray diffraction. The Sr isotope composition of the earliest part (sample 189-7a) of the vein was 0.709941 ± 0.000007, which overlaps the values in the VR1 cements suggesting that carbonate was similarly sourced from dissolving GEG shell carbonate or limestones (Fig. 8). These temperatures indicate that both generations of vein calcite formed after the dyke had cooled substantially from its emplacement temperature; they are also cooler than the maximum cementation temperatures reached during VR1 (Z2) cementation. The pore fluid $\delta^{18}O$ values are consistent with a fracture-fed source from isotopically negative Paleocene meteoric water that had undergone relatively low interaction (high water/rock ratio) with host rocks. The presence of smectite suggests that the water interacted with some silicate during transit, either rocks of basaltic composition or mudstones in the overlying GEG, and it may be associated with intrusion of the Little Minch Sill Complex which post-dated lava emplacement (Gibson, 1990; Gibson and Jones, 1991; Fowler et al., 2004). Sample 189-6 (Table 1) was taken from the dyke margin in contact with the host sandstone and gave the coolest temperatures (24 ± 8 °C) for this locality, and the most negative pore fluid value (–16.5 ± 1.6‰ VSMOW). This fracture was clearly cemented after cooling of the lava pile.

A vein-fed sample of pure sparry calcite drilled from cemented shelter porosity within articulated *Neomiodon* shells in a limestone (189-8spar; *ex situ* block derived from ~10–20 m above VR1 in inaccessible part the Valtos cliffs; Table 1) gave a $\Delta_{47}$ temperature of 42 ± 6 °C and a $\delta^{18}O_{FLUID}$ value of –14.5 ± 1.1‰ VSMOW. These results are essentially identical to those from a fourth post-cementation vein sample (18-4bulk; Table 1), a ferroan sparry calcite with $\Delta_{47}$ temperature of 40 ± 9 °C and a $\delta^{18}O_{FLUID}$ values of –14.2 ± 1.6‰ VSMOW. Cathodoluminescence characteristics suggest these cements (vug and vein fill) were the same phase (Paxton 2022), the cooler temperatures confirming their formation after the main phase of post-compactional limestone cementation (Hudson and Andrews 1987), probably later in the Paleocene after a period of cooling. The fluid compositions are in keeping with other assumed Paleocene meteoric water sourced values measured in this study (see Table 1 and Fig. 7).

On Eigg we also studied nodular cements sampled from a distinct, 60 cm wide zone of cementation adjacent to a Paleocene dyke (Fig. 4). This sample, taken from the fully cemented horizon (see description in Hudson and Andrews, 1987) within a few centimetres of the dyke margin, gave a $\Delta_{47}$ temperature of 42 ± 9 °C, and a derived $\delta^{18}O_{FLUID}$ value of –14.6 ± 1.7‰ VSMOW. In the past it has been assumed that this zone of cementation was related to the intense contact heating from the dyke (Hudson and Andrews, 1987), an interpretation apparently supported by very negative calcite $\delta^{18}O$ values (–13.8‰ and –17.2‰; Wilkinson, 1992). However, the $\Delta_{47}$ temperatures show that these cements precipitated from warm fluids with a negative, Paleocene, meteoric water composition. This later zone of cementation is thus not related to contact heating effects, but rather to the palaeohydrology of the zone adjacent to the dyke, with cementation focused along the dyke wall (a vertical aquitard). The temperature and fluid composition of this calcite is within the range of the calcites from veins associated with the dyke at Valtos.

Considered together, these vein-related samples demonstrate a range of temperatures and water/rock interaction, the latter controlled by fracture geometry and connectivity. It is likely that the hotter fluids were introduced first, possibly the final phase of basinal fluid contribution, although some heating at Valtos may have post-dated the Skye Lava Group, related to intrusion of the Little Minch Sill Complex, which is well developed in this part of Trotternish (Gibson and Jones, 1991; Schofield et al., 2016). Vein calcites with temperatures below 40 °C are much cooler than the lowest Trotternish AFTA maximum burial temperature of 85°C (Holford et al., 2010) and cooler than a more conservative estimate of maximum burial temperature. For example a mean upper crustal geothermal gradient of 30 °C $km^{-1}$ (as used by Hudson and Andrews 1987) would require maximum temperatures of at least 50 °C (assuming 20 °C surface temperature). We thus

interpret these cooler temperatures to represent mineralization during basin inversion, a rapid erosional process that was probably completed <1 myr after lava emplacement (based on the 0.53±0.23 myr erosion figure established for completely unroofing the Rum Igneous centre; Chambers et al., 2005). The strongly negative $\delta^{18}O_{FLUID}$ compositions of the calcite veins concur with a Paleocene timing for such rapid erosion (see below).

Concretion initiation and growth rate

A summary of the main data trends and our interpretation is given in Figure 9. It is not clear what initiated concretion growth. Zone 1 cementation in VR1 is, so far, unique; cements with similar geochemistry are not known outside Trotternish and may be rare even at the type section (VR2 of Wilkinson (1993) lacks Z1). Despite this, Z1 in VR1 appears to record the first ingress of Paleocene meteoric water into the Valtos sandstone, crucial in constraining the timing of cement growth initiation. Moreover, the Z1 fluid seems to be the first record of substantial pore-water renewal since deposition, facilitated by early Paleocene surface exposure of the upper part of the sandbody. Substantial Paleocene recharge is consistent with paleofloral data from Mull and Skye (Poulter, 2011) that indicates wet climatic conditions. In all other studied concretions, fluids with geochemical compositions similar to Z2 in VR1 precipitated the first concretionary cements (e.g. VR2 in Wilkinson 1993), interpreted here as precipitates from cross-formational basinal fluids. In all cases the pore-fluid ingress caused dissolution of host sandstone shell carbonate promoting supersaturation of pore-water dissolved carbonate. It may be that concretion nucleation was aided by attainment of a critical (high) temperature in the aquifer pore system; no large concretion records a $\Delta_{47}$-derived temperature below 44 ± 6 °C.

As compaction of the Valtos Sandstone by a significant thickness of lava (up to 1200 m; England, 1994; Emeleus and Bell, 2005) was completed after the concretions formed, the rate of concretion growth can be re-evaluated. Modelling by Wilkinson and Dampier (1990) concluded that a Valtos Sandstone concretion of radius 0.5 m would have taken >6 Ma to form in stationary pore fluids, and ~4 Ma with pore fluids flowing ~5 m $a^{-1}$. Numerous necessary assumptions in the model parameterisation were required, including fluid temperature, fluid composition and pore fluid flow rate. Our new interpretations requires reconsideration of these parameters, notably the change in temperature from an assumed 25 °C (Wilkinson and Dampier 1990) to the increasing temperatures, from ~47 to 70-80 °C, recorded here. The temporal constraints from our new data are: 1) that initiation of VR1 was probably contemporaneous with the earliest (pre-lava) igneous activity on Skye (the Portree Hyaloclastite); and 2) that termination of

growth occurred around (or soon after) the time the Skye Lava Group was fully emplaced. Emplacement of the Skye Lava Group is thought to have occurred within 1.6 Ma (Hamilton et al., 1998), followed, within <1 myr, by rapid erosion (based on Chambers et al., 2005) which removed much of the lava pile and terminated sandstone compaction. Thus concretion growth and final host sandstone compaction must have completed in no more than ~2.6 myr. This implies that concretion growth rate was approximately double the previously modelled fastest value. This does not invalidate the modelling approach but it does demand reconsideration of the parameterisation.

**Hebridean Paleocene Meteoric Water $\delta^{18}O$ Revisited**

The revised (Paleocene) timing of concretion growth onset explains how negative $\delta^{18}O_{carbonate}$ compositions are preserved in the middle of the large concretions during their initial stages (Z1) of growth. These compositions are partly due to the calcite precipitation temperatures but strongly linked to the negative $\delta^{18}O$ composition of Hebridean Paleocene meteoric water around –12‰ VSMOW. If our proposed timing of concretion initiation is correct, it also informs on the mechanism for these strongly negative meteoric water compositions. It has been known since the 1970s that meteoric water with a $\delta^{18}O_{fluid}$ composition around –12‰ VSMOW was involved in hydrothermal reactions around the Paleocene igneous centres (Taylor and Forester, 1971; Forester and Taylor, 1977). It has been inferred that these negative compositions could have resulted from orographic effects (Taylor and Forester, 1971; MacDonald et al., 2019) caused by the developing high relief volcanic landscape. However, our timing for concretion initiation, around 60.5 Ma (Hamilton et al., 1998) pre-dates the development of volcanic topography. This implies that the negative compositions mainly derive from the latitude of the Hebridean region at that time, around 45° N according to Ganerød et al. (2010) and Smith et al. (1994). The modern temperature (and concomitant less-negative precipitation $\delta^{18}O$) latitudinal anomaly (Rozanski et al., 1993) over coastal Western Europe is caused by heat from the Gulf Stream/North Atlantic Current. This North Atlantic circulation established after the Paleocene, possibly in the Eocene, there being clear evidence for onset or strengthening of the Atlantic meridional overturning circulation (AMOC) ~34 Ma, at the Eocene-Oligocene Transition (Hutchinson et al., 2019).

A latitudinal explanation for strongly negative Paleocene meteoric water compositions is also consistent with some of the Cretaceous modelling (Poulsen et al., 2007; Suarez et al., 2011) that allow for pre-Paleocene Hebridean meteoric water $\delta^{18}O$ compositions around –10 to –11‰ VSMOW. Furthermore, $\delta^{18}O_{fluid}$ values from the

majority of veins and vugs that post-date concretion growth are even more negative (minimum of –16.5 ± 1.6‰ VSMOW); it is probably these compositions that record an orographic component, driven by the high relief volcanic landscape that had formed by around 58.9 Ma (Hamilton et al., 1999; Bell and Williamson, 2002). For comparison, modern altitude effects on $\delta^{18}O$ in precipitation range from –1.7 to –5.0‰ $km^{-1}$ (global mean –2.8‰ $km^{-1}$; Poage and Chamberlain, 2001). Assuming Hebridean Paleocene volcanic relief around 1200 m, our observed difference of ~4‰ between highest and lowest inferred Paleocene meteoric water $\delta^{18}O$ compositions is comfortably within the modern range for altitude effects.

## Conclusions and Wider Implications

Our results highlight the growing realization that secure chronologies on basinal burial diagenetic cementation is crucial for the correct interpretation of paragenetic evolution based on geochemical data. It has recently proven feasible to radiometrically date suitable calcite cements using U/Pb techniques (Jahn & Cuvellier, 1994; Rasbury & Cole, 2009; Mangenot et al., 2018b; Roberts et al., 2020). However, such dating is difficult in many calcite cemented sandstones due to relatively high common Pb levels or low U/Pb ratios (Su et al., 2022); some Paleogene Hebridean calcites are known to have too little radiogenic Pb to yield an age (MacDonald et al., 2019).

The case of the Valtos Sandstone Formation concretions described here is unusual, probably unique; clumped isotope data, combined with traditional stable isotope and trace element data has enabled an unusually precise understanding of cementation chronology because the cementation timing is genetically related to a Paleocene volcanic history which has been radiometrically dated. Ironically, although the chronology of the Paleocene Igneous Event may still be considered quite poor volcanologically, it provides a relative chronology for cementation history of comparable quality to those based on U/Pb dates (e.g., Hill et al., 2016; Beaudoin et al., 2018; Li et al., 2022).

Our new clumped isotope data show that a number of aspects of previous interpretations about cementation history in the Valtos Sandstone Formation were wrong. The studied concretions were not cemented in the Jurassic, or the Cretaceous (Hudson and Andrews 1987; Wilkinson, 1993), but in the Paleocene. The sandstone aquifer was apparently not significantly renewed by inflowing pore-water for almost 100 myr, a finding that is highly relevant to other sandstone hydrocarbon reservoirs or aquifers. Meteoric water that did access the aquifer was at very shallow burial depth, no more than

100 m. This groundwater was locally recharged, then heated by Paleocene phreato-magmatic (vent) activity. Subsequently this fluid was mixed in the sandstone pore-system with upward flowing basinal fluids. The rapidly growing Paleocene lava pile caused compactional basinal fluid flow and sandstone compaction. The latter may have been in part concurrent with later growing concretions (those with Z2 geochemical characteristics) and may explain why compactional deformation is not obvious around all concretions.

The radiometric dates from the Skye Lava Group show that the concretionary cementation and final compaction was completed in no more than 2.6 myr, far more rapidly than modelled previously (Wilkinson and Dampier, 1990). There is no evidence that the sandstone was a conduit for convection-driven meteoric water emanating from the Skye igneous centre hydrothermal system (Schofield et al., 2016). Such flow would necessarily have post-dated concretion formation but there is no record of it in the Valtos Formation or in the older Bearreraig Sandstone (Thrasher 1992; Lewis et al., 1992).

The clumped isotope data also demonstrate that paragenetic histories based on geochemical data where assumptions have been made about burial temperatures and/or pore fluid $\delta^{18}O$ compositions should be regarded as insecure. Our new discoveries were unexpected and have forced us to re-think the burial diagenetic and geological history of rocks we thought we understood. Until now we have missed the significance of Paleocene volcanic rocks resting on an erosive contact with underlying GEG rocks. It had been concluded (Hudson and Andrews 1987) that the GEG rocks had largely completed their sedimentary diagenesis long before the arrival of Paleocene lavas. The possibility that the Valtos Formation sandstones were a high permeability conduit that briefly transmitted hot, meteoric-sourced, shallow groundwater in the Paleocene was not considered. We now know that cement temperatures >50 °C in the GEG mainly come from the large concretions of the Valtos Sandstone Formation: cement temperatures >50 °C are uncommon in mudstone-dominated units (Lealt Shale and Duntulm Formations; Fig. 1) above and below the sandstone (Paxton 2022); these acted largely as aquitards, with fluid flow restricted to faults, fractures and thin permeable sandy beds. The mudstone-dominated formations thus preserve the most reliable record of the overall GEG burial conditions, albeit with temperatures only estimated at ~50-60 °C. The Valtos sandstone records a brief period hydrothermal/basinal fluid temperatures >50 °C and <100 °C during the Paleocene.



**Acknowledgments**

Core plugs from VR1 were collected by Mark Wilkinson and made available from the Leicester University archive collection by Vicky Ward, who also provided thin sections of the plugs. Eileen Gallagher and Matt Wakefield provided additional samples, in particular basalt from the Eigg Lava Formation, collected from the south-west side of Laig Bay. RP was in receipt of a NERC studentship (NE/L002582/1) through the ENVEAST Doctoral Training Partnership at UEA. We thank John Hudson, Brian Bell, Tom Anderson and John Faithful for helpful suggestions and discussion; Mark Wilkinson and an anonymous reviewer gave helpful comments on the manuscript.

## References

ANDERSON, F. W. & DUNHAM, K. C. 1966. *The geology of northern Skye*, HM Stationery Office.

ANDERSON, T. F. & ARTHUR, M. A. 1983. Stable isotopes of oxygen and carbon and their application to sedimentologic and paleoenvironmental problems. In Arthur, M.A., Anderson, T. F. Kaplan, I. R. Veizer J. & Land L. S. (eds) *Stable Isotopes in Sedimentary Geology*, Society of Economic Palaeontologists and Mineralogist Short Course Notes. No. 10, p. 1.1-1.151. Tulsa, Oklahoma.

ANDREWS, J. E. 1986. Microfacies and geochemistry of Middle Jurassic algal limestones from Scotland. *Sedimentology,* 33**,** 499-520.

ANDREWS, J. E., HAMILTON, P. J. & FALLICK, A.E., 1987. The geochemistry of early diagenetic dolostones from a low-salinity Jurassic lagoon. *Journal of the Geological Society,* 144**,** 687-698.

BEAUDOIN, N., LACOMBE, O., ROBERTS, N. M. W. & KOEHN, D. 2018. U-Pb dating of calcite veins reveals complex stress evolution and thrust sequence in the Bighorn Basin, Wyoming, USA. *Geology*, 46, 1015-1018.

BELL, B. R. & WILLIAMSON, I. T. 2002. Tertiary Igneous Activity. *In:* TREWIN, N. H. (ed.) *The Geology of Scotland.* 4th Edition ed. London: The Geological Society, London, 371-407.

BERGMAN, S. C., HUNTINGTON, K. W. & CRIDER, J. G. 2013. Tracing paleofluid sources using clumped isotope thermometry of diagenetic cements along the Moab Fault, Utah. *American Journal of Science,* 313**,** 490-515.

BERNASCONI, S. M., MÜLLER, I. A., BERGMANN, K. D., BREITENBACH, S. F., FERNANDEZ, A., HODELL, D. A., JAGGI, M., MECKLER, A. N., MILLAN, I. & ZIEGLER, M. 2018. Reducing uncertainties in carbonate clumped isotope analysis through consistent

carbonate-based standardization. *Geochemistry, Geophysics, Geosystems,* 19**,** 2895-2914.

BISHOP, A. N. & ABBOTT, G. D. 1995. Vitrinite reflectance and molecular geochemistry of Jurassic sediments: the influence of heating by Tertiary dykes (northwest Scotland). *Organic Geochemistry,* 22**,** 165-177.

BJØRKUM, P. A. & WALDERHAUG, O. 1990. Geometrical arrangement of calcite cementation within shallow marine sandstones. *Earth-Science Reviews,* 29**,** 145-161.

BUDD, D. A., FROST, E. L., HUNTINGTON, K. W. & ALLWARDT, P. F. 2013. Syndepositional deformation features in high-relief carbonate platforms: long-lived conduits for diagenetic fluids. *Journal of Sedimentary Research,* 83**,** 12-36.

CAO, B., LUO, X., WANG, X., ZHANG, L. & SHI, H. 2023. Calcite-cemented concretions in non-marine sandstones: an integrated study of outcrop sedimentology, petrography and clumped isotopes. *Sedimentology*, doi: 10.1111/sed.13071.

CATHLES, L. M. & ADAMS, J. J. 1983. Fluid flow and petroleum and mineral resources in the upper (<20 km) continental crust. In: Jeffrey W. Hedenquist; John F. H. Thompson; Richard J. Goldfarb; Jeremy P. Richards (eds) *Economic Geology, One Hundredth Anniversary Volume*, Society of Economic Geology, doi.org/10.5382/AV100.05.

CATHLES, L. M. & SMITH, A. T. 1983. Thermal constraints on the formation of Mississippi Valley-type lead-zinc deposits and their implications for episodic basin dewatering and deposit genesis. *Economic Geology*, 78, 983–1002.

CHAMBERS, L., PRINGLE, M. & PARRISH, R. R. 2005. Rapid formation of the Small Isles Tertiary centre constrained by precise 40Ar/39Ar and U–Pb ages. *Lithos,* 79**,** 367-384.

CRAIG, H. 1963. The Isotopic geochemistry of water and carbon in geothermal areas, nuclear geology on geothermal areas. *Spoleto 1963***,** 17-53.

CRAIG, H. 1965. The measurement of oxygen isotope paleotemperatures. *Stable isotopes in oceanographic studies and paleotemperatures: Consiglio Nazionale delle Richerche***,** 161-182.

CUI, J., LI, S., & MAO, Z. 2019. Oil-bearing heterogeneity and threshold of tight sandstone reservoirs: A case study on Triassic Chang7 member, Ordos Basin. *Marine and Petroleum Geology*, 104, 180-189.

CUI, J., & LIU, Y. 2021. Determination of Formation Time of Calcareous Cements in Marine

Sandstone and Their Influence on Hydrocarbon Accumulation: A Case Study of the Carboniferous Donghe Sandstone in the Hadexun Oilfield, Tarim Basin. *Geofluids*, 2021(3), 1-15.

DAËRON, M., DRYSDALE, R. N., PERAL, M., HUYGHE, D., BLAMART, D., COPLEN, T. B., LARTAUD, F. & ZANCHETTA, G. 2019. Most Earth-surface calcites precipitate out of isotopic equilibrium. *Nature communications,* 10**,** 429.

DALE, A., JOHN, C. M., MOZLEY, P. S., SMALLEY, P. & MUGGERIDGE, A. H. 2014. Time-capsule concretions: unlocking burial diagenetic processes in the Mancos Shale using carbonate clumped isotopes. *Earth and Planetary Science Letters,* 394**,** 30-37.

DANSGAARD, W. 1964. Stable isotopes in precipitation. *Tellus,* 16**,** 436-468.

DEFLIESE, W. F. & LOHMANN, K. C. 2016. Evaluation of meteoric calcite cements as a proxy material for mass-47 clumped isotope thermometry. *Geochimica et Cosmochimica Acta,* 173**,** 126-141.

DENNIS, P. F., MYHILL, D. J., MARCA, A. & KIRK, R. 2019. Clumped isotope evidence for episodic, rapid flow of fluids in a mineralized fault system in the Peak District, UK. *Journal of the Geological Society,* 176**,** 447-461.

DRAKE, S.M., BEARD, A.D., JONES, A.P., BROWN, D.J., FORTES, A.D., MILLAR, I.L., CARTER, A., BACA, J. & DOWNES, H. 2018. Discovery of a meteoritic ejecta layer containing unmelted impactor fragments at the base of Paleocene lavas, Isle of Skye, Scotland. *Geology*, **46**, 171–174.

EMELEUS, C. H., BELL, B. R. & STEPHENSON, D. 2005. *The Palaeogene volcanic districts of Scotland*, British Geological Survey Nottingham.

ENGLAND, R. W. 1994. The structure of the Skye lava field. *Scottish Journal of Geology,* 30**,** 33-37.

EPSTEIN, S., BUCHSBAUM, R., LOWENSTAM, H. A. & UREY, H. C. 1953. Revised carbonate-water isotopic temperature scale. *Geological Society of America Bulletin,* 64**,** 1315-1326.

FAN, M., HOUGH, B. G., & PASSEY, B. H. 2014. Middle to late Cenozoic cooling and high topography in the central Rocky Mountains: Constraints from clumped isotope geochemistry. *Earth and Planetary Science Letters*, 408, 35-47.

FALLICK, A. E., JOCELYN, J., DONNELLY, T., GUY, M. & BEHAN, C. 1985. Origin of agates in volcanic rocks from Scotland. *Nature,* 313**,** 672-674.

FORESTER, R. W. & TAYLOR, H. P. 1977. $^{18}O/^{16}O$, D/H, and $^{13}C/^{12}C$ studies of the Tertiary

igneous complex of Skye, Scotland. *American Journal of Science,* 277**,** 136-177.

FOWLER, S. J., BOHRSON, W. A. & SPERA, F. J. 2004. Magmatic evolution of the Skye igneous centre, western Scotland: modelling of assimilation, recharge and fractional crystallization. *Journal of Petrology,* 45**,** 2481-2505.

FYFE, L.-J. C., SCHOFIELD, N., HOLFORD, S., HARTLEY, A., HEAFFORD, A., MUIRHEAD, D. & HOWELL, J. 2021. Geology and petroleum prospectivity of the Sea of Hebrides Basin and Minch Basin, offshore NW Scotland. *Petroleum Geoscience,* 27**,** petgeo2021-003.

GANERØD, M., SMETHURST, M., TORSVIK, T., PRESTVIK, T., ROUSSE, S., MCKENNA, C., VAN HINSBERGEN, D. & HENDRIKS, B. 2010. The North Atlantic Igneous Province reconstructed and its relation to the plume generation zone: the Antrim Lava Group revisited. *Geophysical Journal International,* 182**,** 183-202.

GARRELS, R. & CHRIST, C. L. 1965. Solutions, Minerals and Equilibria, Haper & Row. *New York*.

GHOSH, P., ADKINS, J., AFFEK, H., BALTA, B., GUO, W., SCHAUBLE, E. A., SCHRAG, D. & EILER, J. M. 2006. 13C–18O bonds in carbonate minerals: a new kind of paleothermometer. *Geochimica et Cosmochimica Acta,* 70**,** 1439-1456.

GIBSON, S. A. 1990. The geochemistry of the Trotternish sills, Isle of Skye: crustal contamination in the British Tertiary Volcanic Province. *Journal of the Geological Society,* 147**,** 1071-1081.

GIBSON, S. A. & JONES, A. P. 1991. Igneous stratigraphy and internal structure of the Little Minch sill complex, Trotternish Peninsula, northern Skye, Scotland. *Geological Magazine,* 128**,** 51-66.

GUO, W., MOSENFELDER, J. L., GODDARD III, W. A. & EILER, J. M. 2009. Isotopic fractionations associated with phosphoric acid digestion of carbonate minerals: insights from first-principles theoretical modeling and clumped isotope measurements. *Geochimica et Cosmochimica Acta,* 73**,** 7203-7225.

GUO, Y., DENG, W., LIU, X., KONG, K., YAN, W. & WEI, G. 2021. Clumped isotope geochemistry of island carbonates in the South China Sea: Implications for early diagenesis and dolomitization. *Marine Geology,* 437**,** 106513.

HAMILTON, M., PEARSON, D., THOMPSON, R., KELLEY, S. & EMELEUS, C. 1998. Rapid eruption of Skye lavas inferred from precise U–Pb and Ar–Ar dating of the Rum and Cuillin plutonic complexes. *Nature,* 394**,** 260-263.

HAMILTON, P. J., FALLICK, A.E., ANDREWS, J.E. & WHITFORD, D.J. 1992. Middle Jurassic

clay-minerals from the Minch Basin: isotopic tracing of provenance and post-depositional alteration. In: Parnell, J. (ed.) *Basins of the Atlantic Seaboard: Petroleum Geology, Sedimentology and Basin Evolution*. Geological Society, London, Special Publication, 62**,** 155-158.

HAQ, B. U. 2014. Cretaceous eustasy revisited. *Global and Planetary change,* 113**,** 44-58.

HARKER, S.D. 2002. Cretaceous. *In:* TREWIN, N. H. (ed.) *The Geology of Scotland.* 4th Edition ed. London: The Geological Society, London, 351-360

HARRIS, J.P. 1989. The sedimentology of a Middle Jurassic lagoonal delta system: Elgol Formation (Great Estuarine Group), NW Scotland. In: Whateley, M.K.G. & Pickering, K.T. (eds) *Deltas: Sites and Traps for Fossil Fuels*, Geological Society, London, Special Publication, **41,** 147-166.

HARRIS, J. P. 1992. Mid-Jurassic lagoonal delta systems in the Hebridean basins: thickness and facies distribution patterns of potential reservoir sandbodies. In: Parnell, J. (ed.) Basins of the Atlantic Seaboard: Petroleum Geology, Sedimentology and basin Evolution. *Geological Society, London, Special Publication,* 62**,** 111-144.

HARRIS, J.P. & HUDSON, J.D. 1980. Lithostratigraphy of the Great Estuarine Group (Middle Jurassic), Inner Hebrides. *Scottish Journal of Geology,* 16**,** 231-250.

HEIMHOFER, U., MEISTER, P., BERNASCONI, S. M., ARIZTEGUI, D., MARTILL, D. M., RIOS-NETTO, A. M. & SCHWARK, L. 2017. Isotope and elemental geochemistry of black shale-hosted fossiliferous concretions from the Cretaceous Santana Formation fossil Lagerstätte (Brazil). *Sedimentology,* 64**,** 150-167.

HEMINGWAY, J. D. & HENKES, G. A. 2021. A disordered kinetic model for clumped isotope bond reordering in carbonates. *Earth and Planetary Science Letters,* 566**,** 116962.

HENDRY, J. P. 1993. Geological controls on regional subsurface carbonate cementation: an isotopic-paleohydrologic investigation of Middle Jurassic Limestones in central England. In: A.D. Horbury & A.G. Robinson (eds). Diagenesis and Basin Development, AAPG Studies in Geology, No. 36, The American Association of Petroleum Geologists, Tulsa, p. 231-60.

HENKES, G. A., PASSEY, B. H., GROSSMAN, E. L., SHENTON, B. J., PÉREZ-HUERTA, A. & YANCEY, T. E. 2014. Temperature limits for preservation of primary calcite clumped isotope paleotemperatures. *Geochimica et Cosmochimica Acta,* 139**,** 362-382.

HESSELBO, S.P., OATES, M.J. & JENKYNS, H.C. 1998. The Lower Lias Group of the Hebrides Basin. *Scottish Journal of Geology*, **34**, 23-60.

HILL, C. A., POLYAK, V. J., ASMEROM, Y. & PROVENCIO, P. 2016. Constraints on a Late Cretaceous uplift, denudation, and incision of the Grand Canyon region, southwestern Colorado Plateau, USA, from U-Pb dating of lacustrine limestone. Tectonics, 35, 896-906.

HOLFORD, S. P., GREEN, P. F., HILLIS, R. R., UNDERHILL, J. R., STOKER, M. S. & DUDDY, I. R. 2010. Multiple post-Caledonian exhumation episodes across NW Scotland revealed by apatite fission-track analysis. *Journal of the Geological Society,* 167**,** 675-694.

HOLMDEN, C. & HUDSON, J. D. 2003. $^{87}Sr/^{86}Sr$ and Sr/Ca Investigation of Jurassic mollusks from Scotland: Implications for paleosalinities and the Sr/Ca ratio of seawater. *Geological Society of America Bulletin,* 115**,** 1249-1264.

HUDSON, J. D. 1963. The ecology and stratigraphical distribution of the invertebrate fauna of the Great Estuarine Series. *Palaeontology,* 6**,** 327-348.

HUDSON, J. D. 1964. The petrology of the sandstones of the Great Estuarine Series and the Jurassic palaeogeography of Scotland. *Proceedings of the Geologists' Association,* 75**,** 499-527.

HUDSON, J. D. 1980. Aspects of brackish-water facies and faunas from the Jurassic of north-west Scotland. *Proceedings of the Geologists' Association,* 91**,** 99-105.

HUDSON, J. D. 1983. Mesozoic sedimentation and sedimentary rocks in the Inner Hebrides. *Proceedings of the Royal Society of Edinburgh, Section B: Biological Sciences,* 83**,** 47-63.

HUDSON, J. D. & ANDREWS, J. E. 1987. The diagenesis of the Great Estuarine Group, Middle Jurassic, Inner Hebrides, Scotland. *Geological Society, London, Special Publications,* 36**,** 259-276.

HUDSON, J.D. & HARRIS, J. P. 1979. Sedimentology of the Great Estuarine Group (Middle Jurassic) of north-west Scotland. Symp. Sédimentation Jurassique W. Européen, Paris, 1977. *Assoc. Sédimentol. Fr*.

HUNTINGTON, K. W., BUDD, D. A., WERNICKE, B. P. & EILER, J. M. 2011. Use of clumped-isotope thermometry to constrain the crystallization temperature of diagenetic calcite. *Journal of Sedimentary Research,* 81**,** 656-669.

HUTCHINSON, D.K., COXALL, H.K., O'REGAN, M., NILSSON, J., CABALLERO, R. & DE BOER, A.M. 2019. Arctic closure as a trigger for Atlantic overturning at the Eocene-Oligocene Transition. *Nature Communications*, 10, 3797.

JAHN, B.-M. & CUVELLIER, H. 1994. Pb-Pb and U-Pb geochronology of carbonate rocks: an

assessment. *Chemical Geology,* 115**,** 125-151.

JIMENEZ-RODRIGUEZ, S., QUADE, J., DETTINGER, M., HUNTINGTON, K. W., & KELSON, J. R. 2022. Comparing isotopic estimates of paleoelevation from carbonates and volcanic glass from the Miocene-age Chucal Formation in northern Chile. *Chemical Geology*, 596, 120798.

KIM, S.-T. & O'NEIL, J. R. 1997. Equilibrium and nonequilibrium oxygen isotope effects in synthetic carbonates. *Geochimica et Cosmochimica Acta,* 61**,** 3461-3475.

KING, P. M. 1976. *The secondary minerals of the tertiary lavas of northern and central Skye-zeolite zonation patterns their origin and formation*, Ph.D thesis, University of Aberdeen.

KIRK, R. 2017. *Development of clumped isotope techniques and their application to palaeoclimate studies.* PhD thesis, University of East Anglia.

LEFORT, A., HAUTEVELLE, Y., LATHUILIÈRE, B. & HUAULT, V. 2012. Molecular organic geochemistry of a proposed stratotype for the Oxfordian/Kimmeridgian boundary (Isle of Skye, Scotland). *Geological Magazine,* 149**,** 857-874.

LEWIS, C. L. E., CARTER, A. & HURFORD, A. J. 1992. Low-temperature effects of the Skye Tertiary intrusions on Mesozoic sediments in the Sea of the Hebrides Basin. In: PARNELL, J. (ed.) Basins on the Atlantic Seaboard. Petroleum Geology, Sedimentology and Evolution. Geological Society, London, Special Publication, 62, 175-188.

LI, G., XU, W., LUO, Y., LIU, J., ZHAO, J., FENG, Y., CHENG, J., SUN, Z., XIANG, R., XU, M. & YAN, W. 2022. Strontium isotope stratigraphy and LA-ICP-MS U-Pb carbonate age constraints on the Cenozoic tectonic evolution of the southern South China Sea. *Geological Society of America Bulletin*, doi.org/10.1130/B36365.1

LOYD, S. J., CORSETTI, F. A., EILER, J. M. & TRIPATI, A. K. 2012. Determining the diagenetic conditions of concretion formation: assessing temperatures and pore waters using clumped isotopes. *Journal of Sedimentary Research,* 82**,** 1006-1016.

LOYD, S. J., DICKSON, J., BOLES, J. R. & TRIPATI, A. K. 2014. Clumped-isotope constraints on cement paragenesis in septarian concretions. *Journal of Sedimentary Research,* 84**,** 1170-1184.

MACDONALD, J., FAITHFULL, J., ROBERTS, N., DAVIES, A., HOLDSWORTH, C., NEWTON, M., WILLIAMSON, S., BOYCE, A. & JOHN, C. 2019. Clumped-isotope palaeothermometry and LA-ICP-MS U–Pb dating of lava-pile hydrothermal calcite veins. *Contributions to Mineralogy and Petrology,* 174**,** 1-15.

MANGENOT, X., GASPARRINI, M., ROUCHON, V., & BONIFACIE, M. 2018a. Basin-scale thermal and fluid flow histories revealed by carbonate clumped isotopes ($\Delta_{47}$) – Middle Jurassic carbonates of the Paris Basin depocentre. *Sedimentology*, 65, 123–150.

MANGENOT, X., GASPARRINI, M., GERDES, A., BONIFACIE, M. & ROUCHON, V. 2018b. An emerging thermochronometer for carbonate-bearing rocks: $\Delta_{47}$/(U-Pb). *Geology,* 46**,** 1067-1070.

McBRIDE, E. F. 1988. Contrasting diagenetic histories of concretions and host rock, Lion Mountain Sandstone (Cambrian), Texas. *Geological Society of America Bulletin,* 100**,** 1803-1810.

McBRIDE, E. F., PICARD, M. D. & MILLIKEN, K. L. 2003. Calcite-cemented concretions in Cretaceous sandstone, Wyoming and Utah, USA. *Journal of Sedimentary Research,* 73**,** 462-483.

METHNER, K., MULCH, A., FIEBIG, J., WACKER, U., GERDES, A., GRAHAM, S. A., & CHAMBERLAIN, C. P. 2016. Rapid middle Eocene temperature change in western North America. *Earth and Planetary Science Letters*, 450, 132-139.

MORAD, S., AL-RAMADAN, K., KETZER, J. M. & DE ROS, L. 2010. The impact of diagenesis on the heterogeneity of sandstone reservoirs: A review of the role of depositional facies and sequence stratigraphy. *AAPG bulletin,* 94**,** 1267-1309.

MORTON, N. 1987. Jurassic subsidence history in the Hebrides, NW Scotland. *Marine and Petroleum Geology,* 4**,** 226-242.

MOZLEY, P. S. & BURNS, S. J. 1993. Oxygen and carbon isotopic composition of marine carbonate concretions; an overview. *Journal of Sedimentary Research,* 63**,** 73-83.

NOH, J. H. & LEE, I. 1999. Diagenetic pore fluid evolution in the Pohang Miocene sediments: oxygen isotopic evidence of septarian carbonate concretions and authigenic mineral phases. *Geosciences Journal,* 3**,** 141-149.

NYMAN, S. L., GANI, M. R., BHATTACHARYA, J. P. & LEE, K. 2014. Origin and distribution of calcite concretions in Cretaceous Wall Creek Member, Wyoming: Reservoir-quality implication for shallow-marine deltaic strata. *Cretaceous Research,* 48**,** 139-152.

PASSEY, B. H. & HENKES, G. A. 2012. Carbonate clumped isotope bond reordering and geospeedometry. *Earth and Planetary Science Letters,* 351**,** 223-236.

PAXTON, R. B. 2022. *Clumped isotope geochemistry of British Middle and Upper Jurassic sedimentary archives.* PhD thesis, University of East Anglia.

PAXTON, R. B., DENNIS, P. F., MARCA, A. D., HENDRY, J. P., HUDSON, J. D. & ANDREWS, J.

E. 2021. Taking the heat out of British Jurassic septarian concretions. *The Depositional Record,* 7**,** 333-343.

POAGE, M. A. & CHAMBERLAIN, C. P. 2001. Empirical relationships between elevation and the stable isotope composition of precipitation and surface waters: considerations for studies of paleoelevation change. *American Journal of Science,* 301**,** 1-15.

POPE, E.C., BIRD, D.K., ARNÓRSSON, S., FRIDRIKSSON, TH., ELDERS, W.A. & FRIDLEIFSSON, G.Ó. 2009. Isotopic constraints on ice age fluids in active geothermal systems: Reykjanes, Iceland. Geochimica et Cosmochimica Acta, 73, 4468-4488.

POPE, E.C., BIRD, D.K., ARNÓRSSON, S., FRIDRIKSSON, TH., ELDERS, W.A. & FRIDLEIFSSON, G.Ó. 2010. Iceland Deep Drilling Project (IDDP): Stable Isotope Evidence of Fluid Evolution in Icelandic Geothermal Systems. Proceedings World Geothermal Congress 2010, Bali, Indonesia, 25-29 April, p.1-7.

POULSEN, C. J., POLLARD, D. & WHITE, T. S. 2007. General circulation model simulation of the $\delta^{18}O$ content of continental precipitation in the middle Cretaceous: A model-proxy comparison. *Geology,* 35**,** 199-202.

POULTER, J. J. 2011. *Mid Paleocene fossil floras and climate from western Scotland.* Ph.D thesis, University of Leeds.

PURVIS, K., DENNIS, P., HOLT, L. & MARCA, A. 2020. The origin of carbonate cements in the Hildasay reservoir, Cambo Field, Faroe-Shetland Basin; clumped isotopic analysis and implications for reservoir performance. *Marine and Petroleum Geology*, 104641.

RAISWELL, R. & FISHER, Q. 2000. Mudrock-hosted carbonate concretions: a review of growth mechanisms and their influence on chemical and isotopic composition. *Journal of the Geological Society,* 157**,** 239-251.

RASBURY, E. T. & COLE, J. M. 2009. Directly dating geologic events: U-Pb dating of carbonates. *Reviews of Geophysics,* 47. https://doi.org/10.1029/2007RG000246

ROBERTS, N. M., DROST, K., HORSTWOOD, M. S., CONDON, D. J., CHEW, D., DRAKE, H., MILODOWSKI, A. E., MCLEAN, N. M., SMYE, A. J. & WALKER, R. J. 2020. Laser ablation inductively coupled plasma mass spectrometry (LA-ICP-MS) U–Pb carbonate geochronology: strategies, progress, and limitations. *Geochronology,* 2**,** 33-61.

ROZANSKI, K., ARAGUÁS-ARAGUÁS, L. & GONFIANTINI, R. 1993. Isotopic patterns in modern global precipitation. *Geophysical Monograph-American Geophysical Union,* 78**,** 1-1.

SAMPLE, J. C., TORRES, M. E., FISHER, A., HONG, W.-L., DESTRIGNEVILLE, C., DEFLIESE, W. F. & TRIPATI, A. E. 2017. Geochemical constraints on the temperature and timing of carbonate formation and lithification in the Nankai Trough, NanTroSEIZE transect. *Geochimica et Cosmochimica Acta,* 198**,** 92-114.

SCARROW, J. H. 1992. *Petrogenesis of the Tertiary lavas of the Isle of Skye, NW Scotland.* Ph.D thesis, University of Oxford.

SCHOFIELD, N., JERRAM, D. A., HOLFORD, S., ARCHER, S., MARK, N., HARTLEY, A., HOWELL, J., MUIRHEAD, D., GREEN, P. & HUTTON, D. 2016. Sills in sedimentary basins and petroleum systems. In: Breitkreuz, C., Rocchi, S. (eds) Physical Geology of Shallow Magmatic Systems. Advances in Volcanology. Springer, Cham. https://doi.org/10.1007/11157_2015_17.

SEARL, A. 1992. Sedimentology and early diagenesis of the Broadford Beds (Lower Jurassic), Skye, north-west Scotland. *Geological Journal,* 27**,** 243-270.

SELLES-MARTINEZ, J. 1996. Concretion morphology, classification and genesis. *Earth-Science Reviews,* 41**,** 177-210.

SEYFRIED J.R., W., DING, K. & BERNDT, M. 1991. Phase equilibria constraints on the chemistry of hot spring fluids at mid-ocean ridges. *Geochimica et Cosmochimica Acta,* 55**,** 3559-3580.

SHENTON, B. J., GROSSMAN, E. L., PASSEY, B. H., HENKES, G. A., BECKER, T. P., LAYA, J. C., PEREZ-HUERTA, A., BECKER, S. P. & LAWSON, M. 2015. Clumped isotope thermometry in deeply buried sedimentary carbonates: The effects of bond reordering and recrystallization. *Bulletin,* 127**,** 1036-1051.

SHEPPARD, S. M. F. 1986. Characterization and isotopic variations in natural waters. *Reviews in Mineralogy and Geochemistry,* 16**,** 165-183.

SMITH, A. G., SMITH, D. G. & FUNNELL, B. M. 1994. *Atlas of Mesozoic and Cenozoic coastlines*, Cambridge University Press.

STOLPER, D. A. & EILER, J. M. 2015. The kinetics of solid-state isotope-exchange reactions for clumped isotopes: A study of inorganic calcites and apatites from natural and experimental samples. *American Journal of Science,* 315**,** 363-411.

STOLPER, D. A., EILER, J. M. & HIGGINS, J. A. 2018. Modeling the effects of diagenesis on carbonate clumped-isotope values in deep-and shallow-water settings. *Geochimica et Cosmochimica Acta,* 227**,** 264-291.

SU, A., CHEN, H., FENG, Y.-X. & ZHAO, J.-X. 2022. LA-ICP-MS U-Pb dating and geochemical characterization of oil inclusion-bearing calcite cements: Constraints on primary

oil migration in lacustrine mudstone source rocks. Bulletin, 134, 2022-2036.

SUAREZ, M. B., GONZÁLEZ, L. A. & LUDVIGSON, G. A. 2011. Quantification of a greenhouse hydrologic cycle from equatorial to polar latitudes: the mid-Cretaceous water bearer revisited. *Palaeogeography, Palaeoclimatology, Palaeoecology,* 307**,** 301-312.

SUAREZ, M. B. & PASSEY, B. H. 2014. Assessment of the clumped isotope composition of fossil bone carbonate as a recorder of subsurface temperatures. *Geochimica et Cosmochimica Acta,* 140**,** 142-159.

SWANSON, E. M., WERNICKE, B. P., EILER, J. M. & LOSH, S. 2012. Temperatures and fluids on faults based on carbonate clumped–isotope thermometry. *American Journal of Science,* 312**,** 1-21.

SWART, P.K., CANTRELL, D.L., ARIENZO, M.M. & MURRAY, S.T. 2016. Evidence for high temperature and $^{18}O$-enriched fluids in the Arab-D of the Ghawar Field, Saudi Arabia. *Sedimentology*, 63, 1739-1752.

TAN, F.C. & HUDSON, J. D. 1974. Isotopic studies on the palaeoecology and diagenesis of the Great Estuarine Series (Jurassic) of Scotland. *Scottish Journal of Geology,* 10**,** 91-128.

TAYLOR JR, H. P. & FORESTER, R. W. 1971. Low-$O^{18}$ igneous rocks from the intrusive complexes of Skye, Mull, and Ardnamurchan, Western Scotland. *Journal of Petrology,* 12**,** 465-497.

THRASHER, J. 1992. Thermal effect of the Tertiary Cuillins Intrusive Complex in the Jurassic of the Hebrides: an organic geochemical study. In: Parnell, J. (ed.) *Basins of the Atlantic Seaboard: Petroleum Geology, Sedimentology and Basin Evolution*. Geological Society, London, Special Publication*,* 62**,** 35-49.

WILKINSON, M. 1989. *Sandstone-hosted concretionary cements of the Hebrides, Scotland*, Ph.D thesis, University of Leicester.

WILKINSON, M. 1991. The concretions of the Bearreraig Sandstone Formation: geometry and geochemistry. *Sedimentology,* 38**,** 899-912.

WILKINSON, M. 1992. Concretionary cements in Jurassic sandstones, Isle of Eigg, Inner Hebrides. In: Parnell, J. (ed.) *Basins of the Atlantic Seaboard: Petroleum Geology, Sedimentology and Basin Evolution*. Geological Society, London, Special Publication*,* 62**,** 145-154.

WILKINSON, M. 1993. Concretions of the Valtos Sandstone Formation of Skye: geochemical indicators of palaeo-hydrology. *Journal of the Geological Society,* 150**,**

57-66.

WILKINSON, M. & DAMPIER, M. D. 1990. The rate of growth of sandstone-hosted calcite concretions. *Geochimica et Cosmochimica Acta,* 54**,** 3391-3399.

ZHOU, J., POULSEN, C., POLLARD, D. & WHITE, T. 2008. Simulation of modern and middle Cretaceous marine δ18O with an ocean-atmosphere general circulation model. *Paleoceanography,* 23.

**Figure captions**

**Figure 1.** Stratigraphy of the Great Estuarine Group, with schematic log for Trotternish (Skye). Black and white scale bar divisions represent ~25 m (after Hudson and Andrews, 1987).

**Figure 2.** Map of the Inner Hebrides adapted from Thrasher (1992) with sampling locations. Red dashed zone shows mapped extent (Forester and Taylor 1977) of hydrothermal influence of the Cuillin/Red Hills Igneous Centres. Blue labels identify localities where Paleocene lava was emplaced directly on the eroded surface of the Valtos Formation. Note that these localities are spread across the depositional basin.

**Figure 3.** a) Large spherical concretions >1 m in diameter at Valtos type section, bed 3 (Harris and Hudson, 1980). b) Concretion from same horizon as (a) showing compaction of host sandstone bedding (best seen on LHS). Notebook is 20 cm long.

**Figure 4.** Differential foreshore erosion has produced an upstanding nodular cemented zone about 0.6 m wide adjacent to a Tertiary dyke that cross cuts the Valtos Sandstone Formation at Laig Bay, Isle of Eigg. The most cemented zone is immediately adjacent to the dyke margin and is itself cross cut by calcite-filled fractures that run parallel to the dyke. Hammer for scale.

**Figure 5.** Simplified burial history of the Great Estuarine Group. The brown envelope shows the complete thickness of the GEG. The plot depicts a theoretical maximum (overestimated) burial as tectonic/erosional disturbances are not accounted for. The pecked lines indicate greater uncertainty post-60 Ma and are a compromise solution from varied data sources. The timing of two phases of uplift and land surface erosion of the GEG is

indicated but depth of erosion is not known. The Valtos Sandstone Formation is positioned in the centre of the GEG envelope.

**Figure 6.** Clumped isotope data for concretion VR1; A) $\delta^{13}C$ and $\delta^{18}O_{CARBONATE}$ values measured by MIRA, compared to those in Wilkinson (1993); B) $\Delta_{47}$-derived temperatures; C) derived $\delta^{18}O_{FLUID}$ values.

**Figure 7.** Clumped isotope data for all Valtos Formation concretions and cements from Skye and Eigg. VC = Valtos Cliffs.

**Figure 8.** Sr isotope data for concretion VR1 and dyke vein 189-7a from Valtos (Trotternish) compared other relevant Sr isotope data. In B, the GEG clay data from the Duntulm Formation (DF) and Kilmaluag Formation (KF) are omitted for ease of comparison. UOM = Upper Ostrea member.

**Figure 9.** Schematic to summarise the main data trends and their interpretation

**Table 1.** Clumped isotope data. All uncertainties are ± 1 standard error of the pooled standard deviation of groups described in the Supplementary Material.

**Table 2.** Sr isotope data from concretion VR1 and vein (189-7a) at Valtos, Trotternish.

**Table 3:** Estimates of meteoric $\delta^{18}O_{WATER}$ values for Middle Cretaceous from modelling at latitudes of ~40-45 °N (approximate Hebridean latitude in Mid Cretaceous; Smith et al., 1994). GCM = General Circulation Model

Figure 1

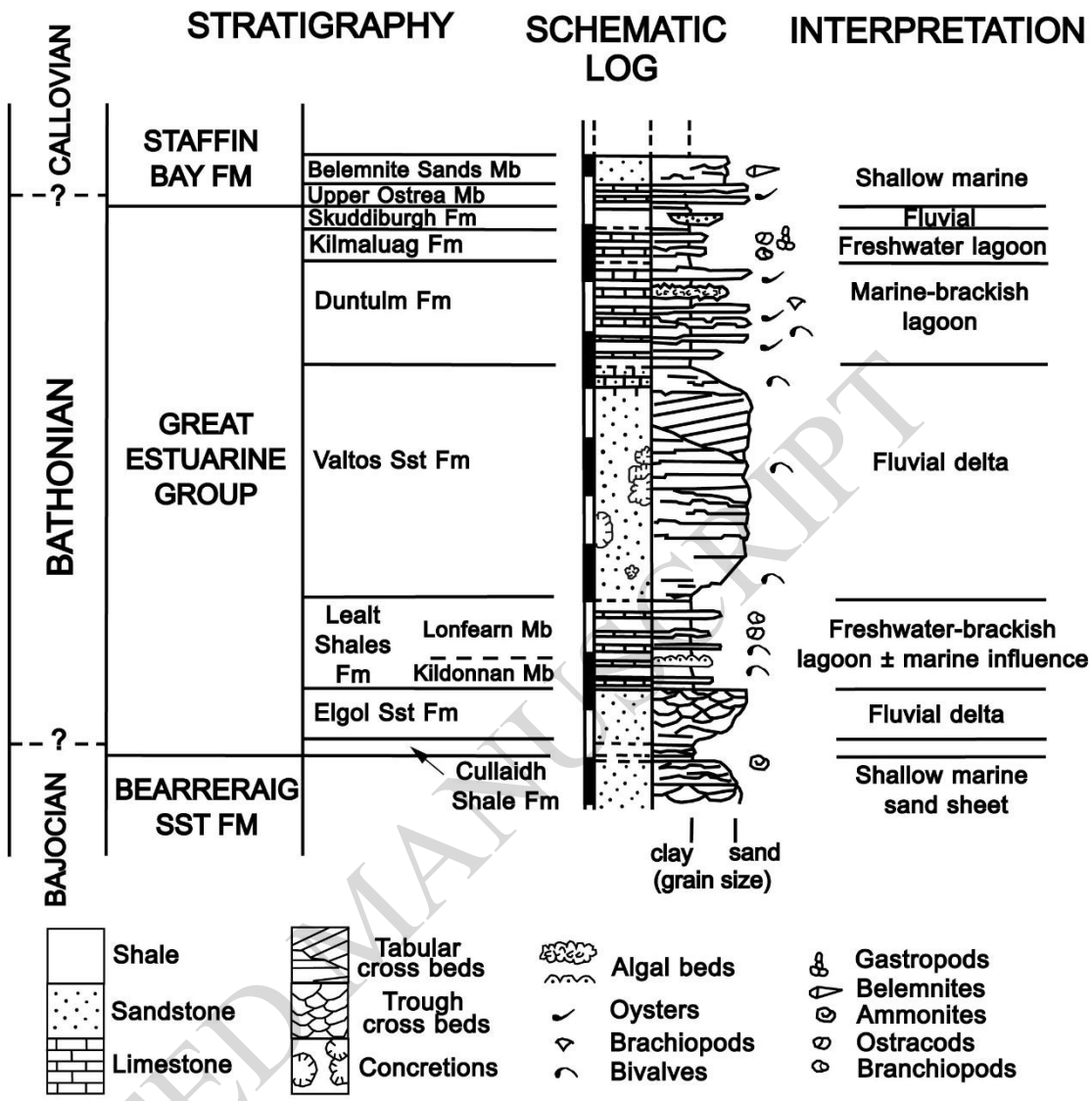

Figure 2

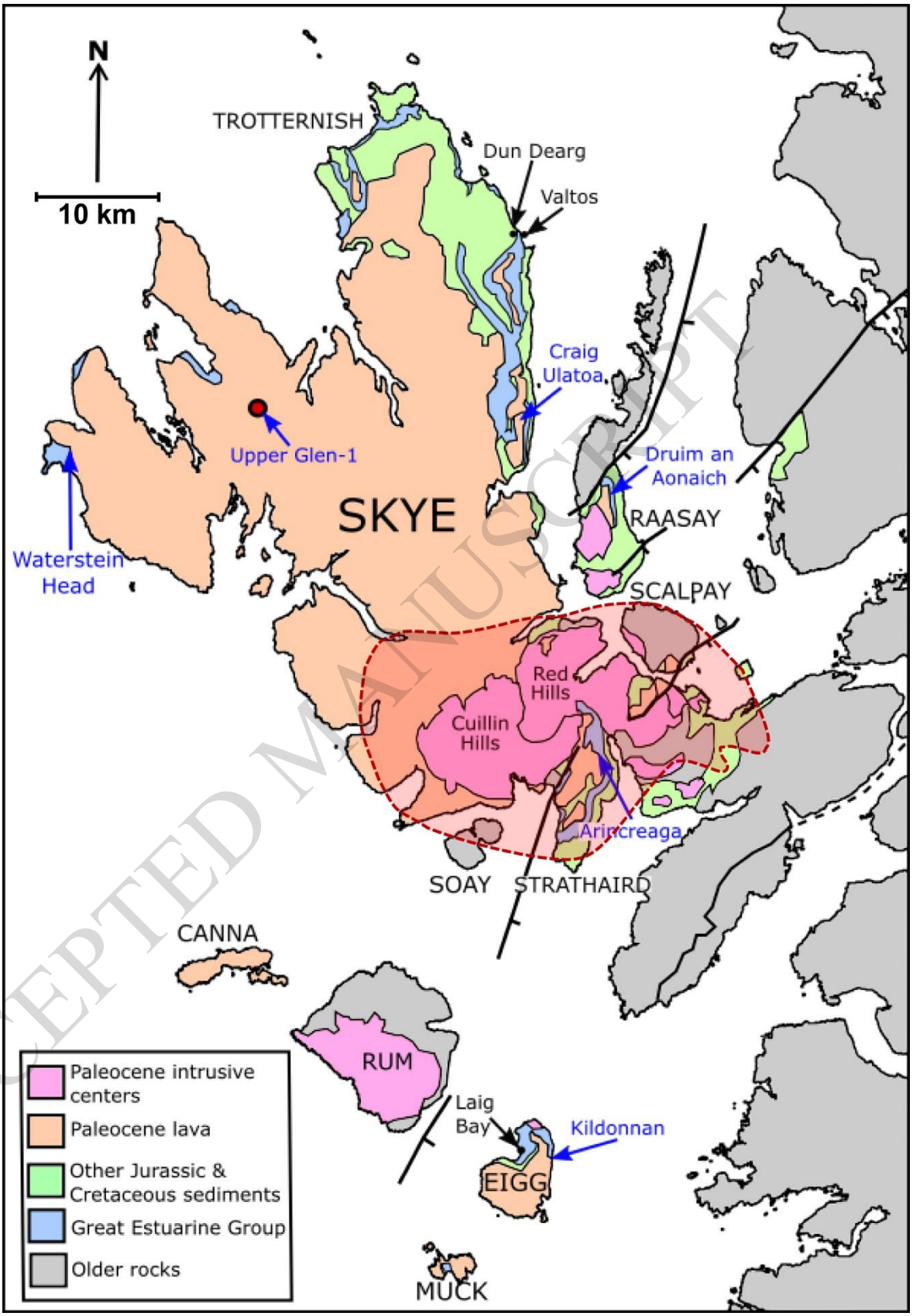

Figure 3

Figure 4

Figure 5

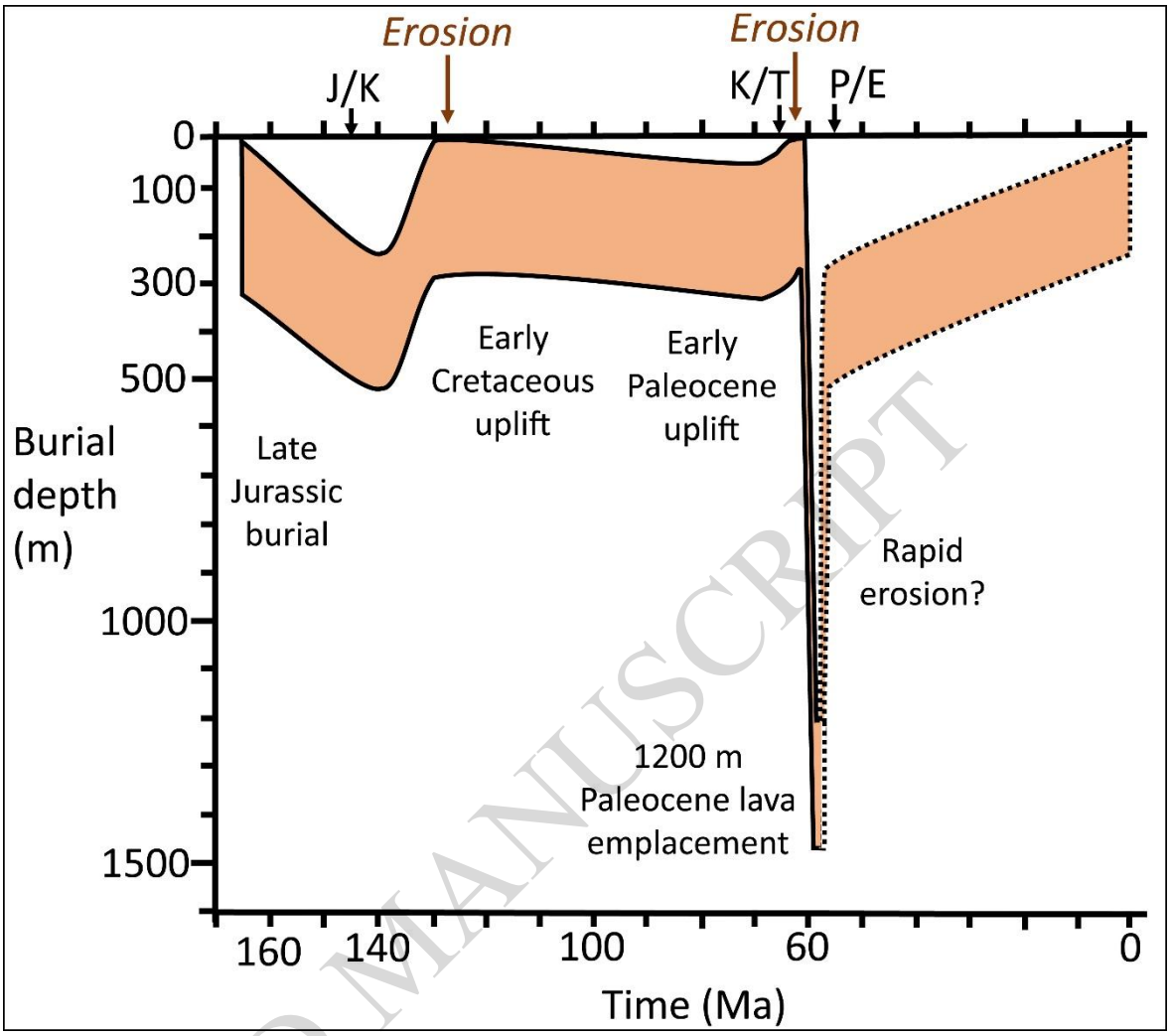

Figure 6

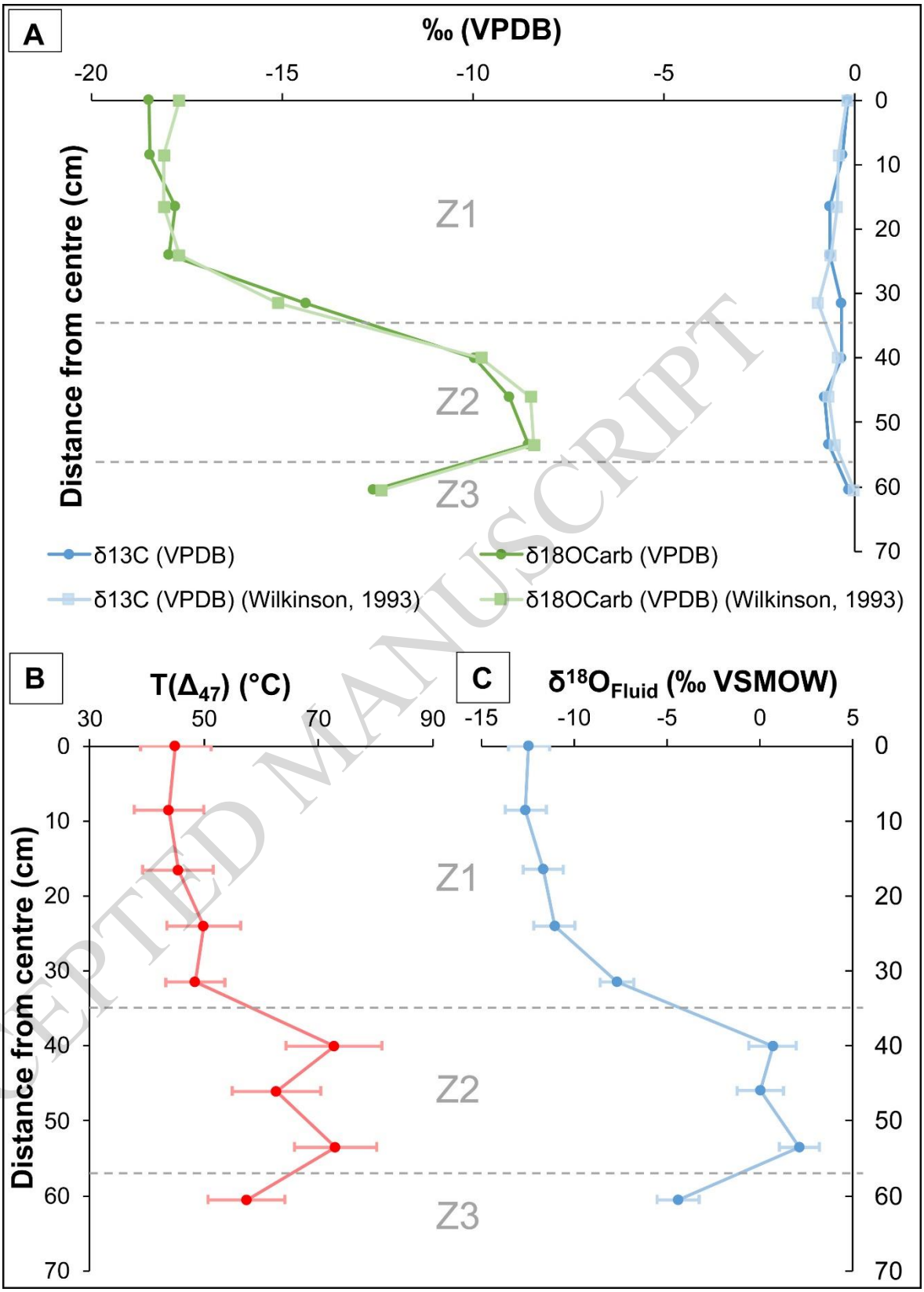

Figure 7

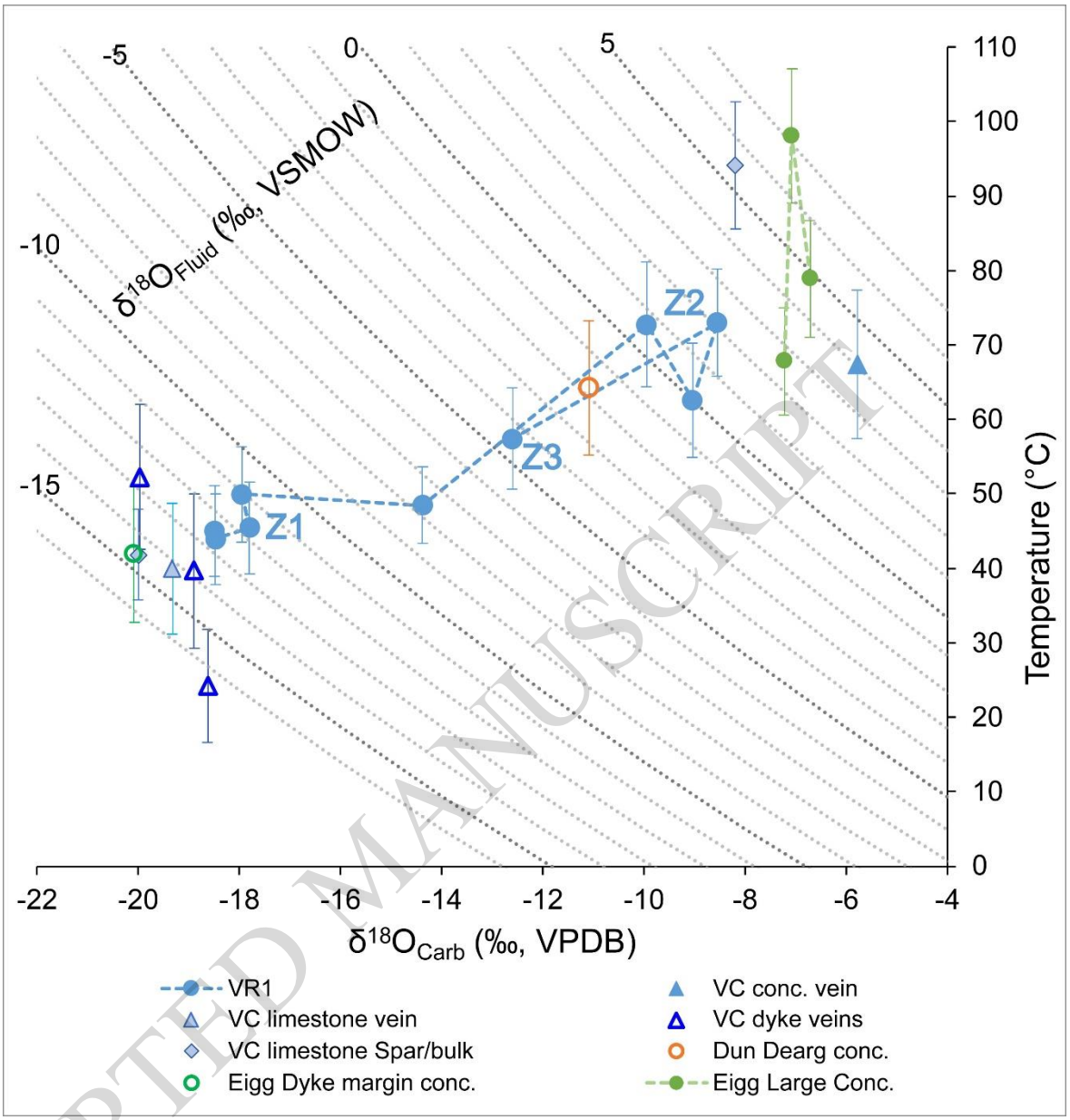

Figure 8

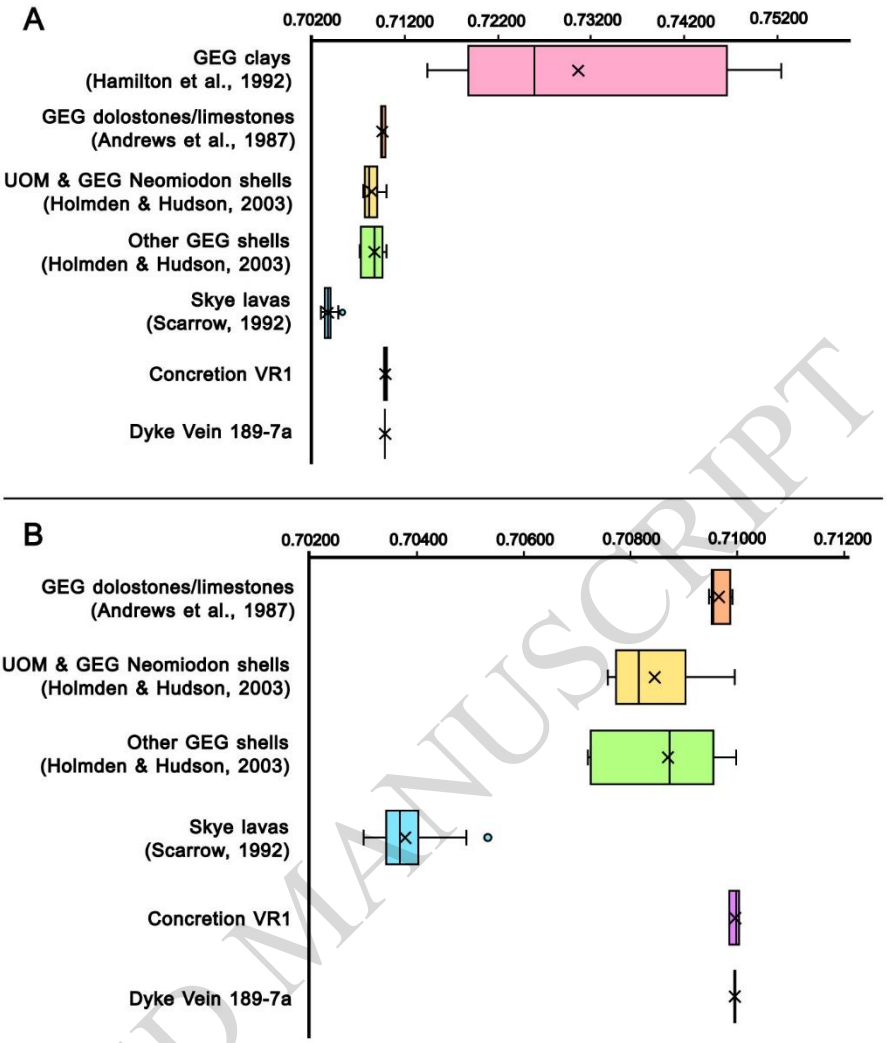

Figure 9

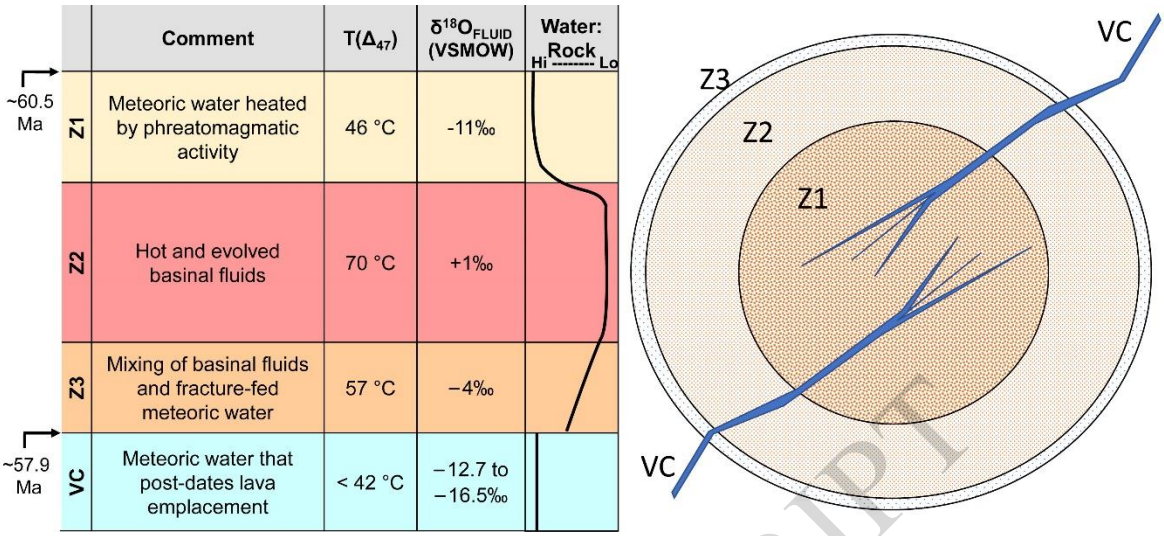

Table 1

| Location | Type | Sample | N | Zone | Distance from centre (cm) | $\delta^{13}C$ (‰, VPDB) | $\delta^{18}O_{CARBONATE}$ (‰, VPDB) | $\Delta_{47}$ (CDES-25) | $T(\Delta_{47})$ (°C) | $\delta^{18}O_{FLUID}$ (‰, VSMOW) |
|---|---|---|---|---|---|---|---|---|---|---|
| Valtos, Skye | Large Sandstone Concretion | M8603 | 4 | Z1 | 0 | -0.19 ± 0.03 | -18.5 ± 0 | 0.598 ± 0.011 | 45 ± 6 | -12.4 ± 1.1 |
| | | M87215 | 4 | | 8.5 | -0.32 ± 0.03 | -18.5 ± 0 | 0.601 ± 0.011 | 44 ± 6 | -12.6 ± 1.1 |
| | | M8604 | 4 | | 16.5 | -0.64 ± 0.03 | -17.8 ± 0 | 0.597 ± 0.011 | 45 ± 6 | -11.7 ± 1.1 |
| | | M87216 | 4 | | 24 | -0.64 ± 0.03 | -18 ± 0 | 0.587 ± 0.011 | 50 ± 6 | -11.1 ± 1.1 |
| | | M8605 | 10 | | 31.5 | -0.35 ± 0.02 | -14.4 ± 0 | 0.59 ± 0.007 | 48 ± 5 | -7.7 ± 0.9 |
| | | M87217 | 3 | Z2 | 40 | -0.35 ± 0.03 | -10 ± 0 | 0.539 ± 0.013 | 73 ± 8 | 0.7 ± 1.3 |
| | | M8606 | 3 | | 46 | -0.8 ± 0.03 | -9 ± 0 | 0.559 ± 0.013 | 63 ± 8 | 0 ± 1.2 |
| | | M87218 | 5 | | 53.5 | -0.67 ± 0.02 | -8.6 ± 0 | 0.539 ± 0.01 | 73 ± 7 | 2.1 ± 1.1 |
| | | M8607 | 4 | Z3 | 60.5 | -0.16 ± 0.03 | -12.6 ± 0 | 0.57 ± 0.011 | 57 ± 7 | -4.4 ± 1.1 |
| Dun Dearg, Skye | Large Sandstone Concretion | EG191015-1 | 2 | | Base | 2.05 ± 0.04 | -11.09 ± 0.04 | 0.556 ± 0.016 | 64 ± 9 | -1.8 ± 1.4 |
| Laig Bay, Eigg | | 169-9 | 3 | | 0 | 1.52 ± 0.04 | -6.72 ± 0.05 | 0.528 ± 0.011 | 79 ± 8 | 4.9 ± 1.1 |
| | | 169-11 | 3 | | 56 | 3.25 ± 0.04 | -7.08 ± 0.05 | 0.496 ± 0.011 | 98 ± 9 | 7.2 ± 1.2 |
| | | 169-10 | 3 | | 80 | 3.08 ± 0.04 | -7.23 ± 0.05 | 0.549 ± 0.011 | 68 ± 7 | 2.7 ± 1.1 |
| | Dyke margin nodule | 169-1r | 3 | | | -0.1 ± 0.02 | -20.08 ± 0.02 | 0.606 ± 0.02 | 42 ± 9 | -14.6 ± 1.7 |
| Valtos, Skye | Calcite Vein | 18-4bulk | 3 | | | 0.06 ± 0.04 | -19.33 ± 0.12 | 0.611 ± 0.02 | 40 ± 9 | -14.2 ± 1.6 |
| | | 189-1 | 4 | | | -0.06 ± 0.03 | -5.79 ± 0.1 | 0.549 ± 0.017 | 67 ± 10 | 4.1 ± 1.5 |
| | | 189-5v | 3 | | | -1.98 ± 0.04 | -19.96 ± 0.12 | 0.581 ± 0.02 | 52 ± 10 | -12.7 ± 1.7 |
| | | 189-6 | 3 | | | 0.08 ± 0.04 | -18.63 ± 0.12 | 0.654 ± 0.02 | 24 ± 8 | -16.5 ± 1.6 |
| | | 189-7a | 2 | | | -3.39 ± 0.05 | -18.9 ± 0.15 | 0.611 ± 0.024 | 40 ± 10 | -13.8 ± 1.9 |
| | Spar infill | 189-8spar | 5 | | | 1.07 ± 0.04 | -20.01 ± 0.07 | 0.606 ± 0.011 | 42 ± 6 | -14.5 ± 1.1 |
| Laig Bay, Eigg | Amygdales | rp-SA-1 | 4 | | | -6.08 ± 0.04 | -16.58 ± 0.07 | 0.643 ± 0.013 | 28 ± 6 | -13.7 ± 1.2 |
| | | rp-SA-2 | 4 | | | -5.84 ± 0.04 | -17.79 ± 0.07 | 0.646 ± 0.013 | 27 ± 6 | -15.1 ± 1.1 |

Table 2

| Sample ID | Description | Distance from centre (cm) | $^{87}Sr/^{86}Sr$ | Error |
|---|---|---|---|---|
| 189-7a | Earliest vein within dyke at Valtos | | 0.709941 | 0.000007 |
| M8603 | Centre sample, VR1 (Z1) | 0 | 0.709836 | 0.000006 |
| M87218 | 2nd outermost sample, VR1 (Z2) | 53.5 | 0.710020 | 0.000008 |
| M8607 | Edge sample, VR1 (Z3) | 60.5 | 0.709961 | 0.000008 |

Table 3

| Reference | $\delta^{18}O_{FLUID}$ (VSMOW) estimate | Description | Notes |
|---|---|---|---|
| Poulsen et al. (2007) | ~-7‰ to -10‰ | Continental precipitation | Atmospheric GCM with transportation and fractionation of water isotopes; four different $CO_2$ concentrations |
| Zhou et al. (2008) | ~-5.5‰ to -7‰ | Precipitation | Ocean-atmosphere GCM with transportation and fractionation of water isotopes |
| Suarez et al. (2011) | -7.5‰ to -11‰ | Groundwater | Groundwater gradients used in precipitation model as proxies for meteoric composition; matched to meteoric $\delta^{18}O$ compositions derived from pedogenic carbonates |